

Thermal and quantum noncondensate particles near the superfluid to Mott insulator transition

Daw-Wei Wang

Physics Department, National Tsing-Hua University, Hsinchu, Taiwan, ROC
Physics Division, National Center for Theoretical Science, Hsinchu, Taiwan, ROC

(Dated: March 16, 2021)

We investigate the finite temperature momentum distribution of bosonic noncondensate particles inside a 3D optical lattice near the superfluid to Mott insulator transition point, treating the quantum fluctuation and thermal fluctuation effects on equal footing. We explicitly address the different momentum (\mathbf{q}) dependence of quasi-particle distribution resulted from thermal and quantum origins: the former scales as $|\mathbf{q}|^{-2}$ and hence is dominant in the small momentum region, while the latter scales as $|\mathbf{q}|^{-1}$ and hence dominant in the large momentum limit. Analytic and semi-analytic results are derived, providing a unique method to determine various properties inside the optical lattice, including temperature, condensate density, coherent length and/or single particle gap etc. Our results also agree with the scaling theory of a quantum XY model near the transition point. Experimental implication of the TOF measurement is also discussed.

I. INTRODUCTION:

The experimental realization of superfluid (SF) to Mott insulator (MI) transition of ultracold atoms [1,2] in an optical lattice has open a new area of strongly correlated physics and lead to many applications to other fields [3]. It is generally believed that when the size of the expanding atom cloud is much larger than the initial size (i.e. a long-time flight after switching off the trapping potential) and if the interaction effect during the expansion can be neglected [4], the TOF image can be interpreted as a momentum distribution function of the initial atom cloud inside the optical lattice. As a result, the sharp interference peaks at zero momentum and Bragg momentum can be understood as a signature of a Bose-Einstein condensation (or superfluidity) while the wider and smaller hump around the peak is then attributed to the non-condensate particles inside the optical lattice. Different from the superfluidity measurement of condensate via vortices in a single parabolic confinement potential [5], the time-of-flight (TOF) absorption image (i.e. the "bi-modal" structure with a "sharp" interference peak in the TOF image) is so far the only experimental measurement to determine the superfluid/condensate density inside the optical lattice [5,6].

However, behind the scenario of "bi-modal" structure of the interference peak, there is an important assumption: only two length scales (or momentum scales) are relevant in the long wavelength limit and their difference can be distinguishable [7]: one is associate with the size of condensate and the other is associate with the thermal wavelength of non-condensate particles. In fact, from experiment point of view, only after the later part (non-condensate particles) has been identified and subtracted from the TOF image spectrum, one can study the properties (i.e. the sharpness, width, or condensate fraction) of the former (condensate) part, which is the key player to determine the many-body phase diagram and has been extensively discussed in recent theoretical and experimental groups [8,9,10,11,12,13,14,15]. To the

best of our knowledge, so far all the experimental data of these non-condensate particles were fitted by a Gaussian type distribution function at finite momentum and the obtained fitting parameter is interpreted as the temperature of bosons inside the optical lattice [2]. This approach may be justified for weakly interacting bosons at finite temperature, but it cannot be reliable near the SF-MI transition point, where the quantum depletion is known significantly enhanced. In other words, near the quantum transition point, there will be at least *three* relevant length scales in the interference peak: The first one is the condensate size as mentioned above, the second one is the thermal wavelength, and the third one is the healing length, which is associate with the interaction effect or quantum depletion. (The lattice constant and the size of Wannier function can be assumed not relevant when investigating a single peak of the interference pattern.) To the best of our knowledge, there is no useful analytical form of the momentum distribution to distinguish the two different contributions (thermal and quantum) of the non-condensate particles near the SF-MI transition point. Exact numerical simulation cannot distinguish these two contribution either [9,14]. Without a justified theory to describe the momentum distribution of non-condensate particles, the measurement and/or determination of the condensate fraction in the interference peak also becomes questionable. Solving such problem and providing a useful theoretical framework is the motivation and the theme of this work.

In this paper, we apply the three-state effective model developed by Altman *et al.* [16] to calculate the finite temperature momentum distribution of quasi-particles near the SF-MI transition, where the quantum fluctuation can be comparable or even stronger than the finite temperature effect. Our results show that (1) in the superfluid regime, the momentum distribution of thermal excited quasi-particles is different from the one of quantum depleted quasi-particles: the former diverges as $|\mathbf{q}|^{-2}$ in the small momentum (\mathbf{q}) limit, while the latter diverges as $|\mathbf{q}|^{-1}$. In other words, the noncondensate

particle is dominated by thermal particles in small momentum regime while it is by quantum depletion in the larger momentum regime. (2) In the weak interacting regime and in the Mott insulator regime, we obtained an analytical result for the momentum distribution at finite temperature, providing the theoretical fitting equations for the TOF image. The obtained equations can be used to calculate various physical properties, like the condensate fraction, temperature, and single particle gap etc. inside the optical lattice. Note that here we just concentrate on the momentum distribution of particles inside the optical lattice, and assume that this distribution can be observed in a long TOF experiment when the interaction effects during the expansion is negligible [4]. For simplicity, we will just consider the uniform system without the inhomogeneous trapping potential.

This paper is organized as following: In Section II we briefly review the system Hamiltonian and the connection between momentum distribution inside the optical lattice and the momentum distribution in free space. The later can be understood as a result of TOF absorption image if assuming no interaction effect during expansion and neglecting the finite size effect [13]. In Section III, we briefly introduce the three state model and its meanfield phase diagram obtained near the SF-MI transition point, both at zero temperature and finite temperature regime. In Section IV, we first study the momentum distribution calculated in the weakly interacting regime, where one can apply Bogoliubov theory to study the general properties of thermal and quantum depleted quasi-particles. In Section VI, we applied the meanfield solution of the three state model to the Mott insulator phase and obtain some analytic form of momentum distribution function at finite temperature regime. Results near the quantum critical point (QCP) of the SF-MI transition are investigated in Section VII. In Section V, we further apply the three-state model to study the momentum distribution in the superfluid side near QCP, both below and above T_c . We then study and compare the momentum distribution near SF-MI transition by using the scaling theory of quantum XY model in Section VIII, and then discuss some issues related to experimental observation. We finally summarize our results in Section X. All the supplementary materials about the details of calculation are in the Appendices.

II. SYSTEM HAMILTONIAN AND MOMENTUM DISTRIBUTION

In this paper, we consider bosonic atoms loaded in a 3D square optical lattice with lattice constant, a . When the lattice strength is sufficiently large, the system can be well described by a single band Hubbard model:

$$H = -J \sum_{\langle \mathbf{R}, \mathbf{R}' \rangle} a_{\mathbf{R}}^\dagger a_{\mathbf{R}'} + \frac{U}{2} \sum_{\mathbf{R}} n_{\mathbf{R}}(n_{\mathbf{R}} - 1) - \mu \sum_{\mathbf{R}} n_{\mathbf{R}}, \quad (1)$$

where $a_{\mathbf{R}}$ is the bosonic field operator at site \mathbf{R} , and $n_{\mathbf{R}} = a_{\mathbf{R}}^\dagger a_{\mathbf{R}}$ is the density operator. J is the single particle tunneling amplitude. U is onsite interaction energy and μ is the chemical potential. For simplicity, we neglect the harmonic trapping potential throughout this paper. Within this single band approximation, we can express a bosonic field operator ($\Psi(\mathbf{r})$) in lattice momentum expansion (see Appendix A): $\Psi(\mathbf{r}) = \sum_{\mathbf{k}}' a_{\mathbf{k}} \Psi_{\mathbf{k}}(\mathbf{r})$, where $a_{\mathbf{k}} = \Omega^{-1/2} \sum_{\mathbf{R}} a_{\mathbf{R}} e^{-i\mathbf{k}\cdot\mathbf{R}}$ with the lattice volume, $\Omega = L^3$ (we assume L lattice sites in each direction). $\Psi_{\mathbf{k}}(\mathbf{r})$ is the Bloch wavefunction function and $\sum_{\mathbf{k}}'$ is the summation of lattice momentum over the first Brillouin Zone (BZ). As a result, the free space momentum distribution, $N(\mathbf{q})$, can be calculated by mapping the field operator into the plane wave basis (see Appendix A), i.e. $N(\mathbf{q}) = \frac{1}{\Omega} \sum_{\mathbf{k}}' n(\mathbf{k}) \left| \tilde{\Psi}_{\mathbf{k}}(\mathbf{q}) \right|^2$, where $\tilde{\Psi}_{\mathbf{k}}(\mathbf{q})$ is the Fourier transform of Bloch wavefunction $\Psi_{\mathbf{k}}(\mathbf{r})$, and $n(\mathbf{k}) = \langle a_{\mathbf{k}}^\dagger a_{\mathbf{k}} \rangle$ is the momentum distribution of the lattice momentum, \mathbf{k} .

When the lattice potential is sufficiently strong, the lowest band Wannier function can be well-approximated by a Gaussian function with width, σ . As a result, the Bloch wavefunction can be easily calculated to be (see Appendix A): $|\tilde{\Psi}_{\mathbf{k}}(\mathbf{q})|^2 = f(\mathbf{k} - \mathbf{q}) |w(\mathbf{q})|^2$, where $f(\mathbf{q}) \equiv \frac{(2\pi)^3}{\Omega} \left| \sum_{\mathbf{R}} e^{i\mathbf{q}\cdot\mathbf{R}} \right|^2 = \frac{(2\pi)^3}{\Omega} \prod_{\alpha} \left| \frac{\sin(Lq_{\alpha}/2)}{\sin(q_{\alpha}/2)} \right|^2$ and $|w(\mathbf{q})|^2 = \frac{\sigma^3}{\pi^{3/2}} e^{-|\mathbf{q}|^2 \sigma^2}$. The momentum distribution measured in the TOF experiment is then just a column integration of $N(\mathbf{q})$ along the z direction, leading to (see Appendix A for details) $N_{\perp}(\mathbf{q}_{\perp}) = \int_{-\infty}^{\infty} dq_z N(\mathbf{q}) \propto \frac{1}{\Omega} \sum_{\mathbf{k}_{\perp}, k_z} ' n(\mathbf{k}) \left| \tilde{\Psi}_{\mathbf{k}_{\perp}}(\mathbf{q}_{\perp}) \right|^2$ upto an overall constant. Note that to derive above expression, we have used the fact that $\sigma_z |k_z| \ll 1$ in most regime of the first BZ. Finally, we note that when the system size is much larger than the lattice constant, $f(\mathbf{q})$ becomes a sharp peaked function at each reciprocal lattice, \mathbf{G}_{\perp} , with width $\sim 2\pi/L$. As a result, the TOF image, $N_{\perp}(\mathbf{q}_{\perp})$, can be further simplified by approximating $f(\mathbf{q}_{\perp})$ to be a delta function at G_{\perp} , and become (see Appendix A)

$$N_{\perp}(\mathbf{q}_{\perp}) \propto \frac{1}{L} \sum_{k_z} ' n(\mathbf{q}_{\perp}, k_z) |w(\mathbf{q}_{\perp})|^2 \sum_{\mathbf{G}_{\perp}} \delta(\mathbf{q}_{\perp} - \mathbf{G}_{\perp}) \propto n_{\perp}(\mathbf{q}_{\perp}) |w(\mathbf{q}_{\perp})|^2 \quad \text{as } \mathbf{q}_{\perp} \sim 0, \quad (2)$$

where $n_{\perp}(\mathbf{q}_{\perp}) \equiv \frac{1}{L} \sum_{k_z} ' n(\mathbf{q}_{\perp}, k_z)$ is the momentum distribution integrated over the z direction.

III. THREE-STATE MODEL AND FINITE TEMPERATURE PHASE DIAGRAM

The phase diagram of the single band Hubbard model has been extensively studied in the literature in the last ten years. In 2D and 3D systems with a square lattice, meanfield phase diagram has been shown to be a very good approximation for the phase boundary

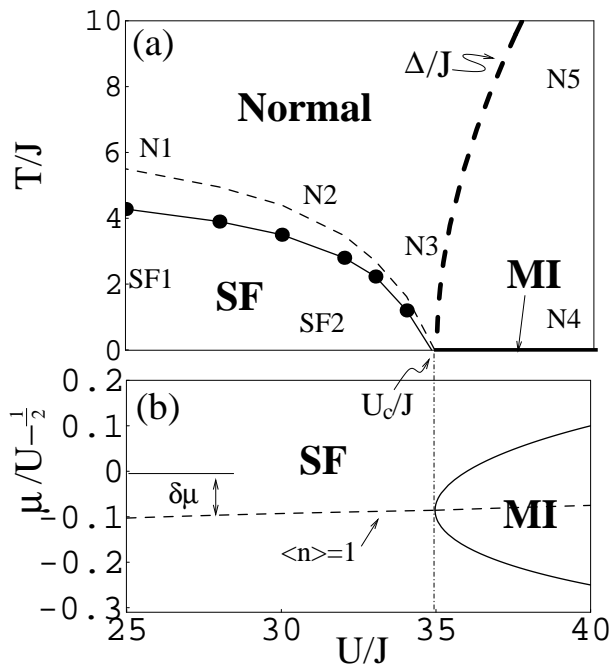


FIG. 1: Meanfield phase diagrams of Bose Hubbard model in a 3D square lattice for $n_0 = 1$: (a) finite temperature phase diagram and (b) quantum phase diagram. The MI lobe in (b) is plotted according to meanfield approximation, with the lobe tip bending down from $U/2$. The horizontal dashed line in (b) indicates the particle-hole symmetric line. The finite temperature phase diagram in (a) is calculated from Eq. (16), and the critical point at $T = 0$ is right the same as the tip position of the MI lobe, as indicated by the vertical dash-dot line. Filled dots are the calculated T_c and the thin line is plotted to guide the eyes. The thin dashed line above T_c is the line of the constant peak width, $k_0 = 0.008\pi/a$, which is the half-width of a Lorentzian fitting function for the momentum distribution. The thick dashed lines is the single particle gap energy in the Mott insulator phase. $N1 \dots N5$, are different regimes of normal state. $SF1$ and $SF2$ are superfluid states in weakly interacting and strongly interacting regime respectively.

[14,19,20,21]. The meanfield study of the SF-MI phase transition can be summarized by the two phase diagrams in Fig. 1(a) and (b), where the quantum critical point, U_c , is defined at the tip of the MI lobe (with average n_0 particle per site) in (b). The finite temperature phase diagram in (a) is obtained by fixing the filling fraction to be an integer, $\langle n_{\mathbf{R}} \rangle = n_0 = 1$. In order to study the momentum distribution in the single band Hubbard model, we separate the study into two regimes: one is the weakly interacting regime of SF phase, and the other is the strongly interacting regime, where superfluid order parameter is very small or even zero when entering the MI regime. For the convenience of later discussion, below we briefly outline the underlying meanfield theories for these two different regimes of phase diagram.

In the weakly interacting regime, i.e. away from the quantum phase transition point in the region $N1$ and $SF1$ of Fig. 1(a), we could apply Bogoliubov-Hartree-

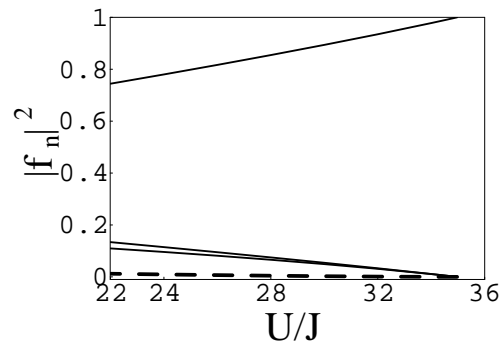


FIG. 2: Probabilities of different number occupation, n , of each lattice site in the superfluid state of unit filling ($n_0 = \langle a_{\mathbf{R}}^{\dagger} a_{\mathbf{R}} \rangle = 1$) at $T = 0$ (see the text). The three solid lines are for $n = 1$, $n = 0$, and $n = 2$ respectively from top to bottom. The dashed line is for $n = 3$, and results for larger number occupation is not visible in this parameter regime.

Fock-Popov approximation to study the quasi-particle excitation and quantum depletion effects both for $T > T_c$ and $T < T_c$. Since this approach has been very well known in the literature [17], we will just outline the results and implication to the momentum distribution in the next section. However, in the second (strongly interacting) regime, we adopt the truncated phase space method developed by Altman *et al.* (Ref. [16]) to study the superfluid phase near the critical point and the Mott insulator phase. Such truncated phase method is justified by using the fact that in the strongly interacting regime, number fluctuation per lattice site can be so small that only three states with number of particles n_0 , $n_0 + 1$, and $n_0 - 1$, are relevant in the low energy regime. In order to verify the validity of such truncated phase space approximation in the superfluid state, we use Gutzwiller trial wavefunction, $|\Psi_{\text{trial}}\rangle = \prod_{\mathbf{R}} (\sum_{n=0}^{\infty} f_n |n\rangle_{\mathbf{R}})$, to calculate the probability of higher number occupation at zero temperature, where $|n\rangle_{\mathbf{R}}$ is the wavefunction for n particles at site \mathbf{R} and f_n is the amplitude of the wavefunction of n particles at each lattice site. By minimizing the total energy of Eq. (1) with a unit filling fraction ($n_0 = 1$) in average, in Fig. 2, we find the probability to have more than two particles per site is very small ($\sim 1\%$, the dashed line) even for $U/J \sim 22$, away from the SF-MI transition point, $U_c/J = 34.97$. Since the transition temperature is also of the same order as the tunneling strength, J , it is reasonable to expect that such truncated phase space method should be justified in a wide range near the SF-MI transition point and at finite temperature not too far away from T_c . In this paper, we will name this truncated phase space scheme to be a three-state model. Since details of the theory have been derived in Ref. [16], below we just listed some important results for completeness and for the convenience of later discussion. Details of the momentum distribution calculation are shown in the Appendix B and C.

In the three-state model, one first truncates the phase

space to $n_0 - 1$, n_0 and $n_0 + 1$ particles per site (with n_0 being the average filling fraction), by defining three bosonic operators, $t_{\alpha,\mathbf{R}}^\dagger$, to be $t_{\alpha,\mathbf{R}}^\dagger|0\rangle = |n_0 + \alpha\rangle_{\mathbf{R}} = \frac{(a_{\mathbf{R}}^\dagger)^{n_0 + \alpha}}{\sqrt{(n_0 + \alpha)!}}|0\rangle$ for $\alpha = 0, \pm 1$. Within this truncated space, a bosonic creation operator can be expressed to be $a_{\mathbf{R}}^\dagger = \sqrt{n_0 + 1}t_{1,\mathbf{R}}^\dagger t_{0,\mathbf{R}} + \sqrt{n_0}t_{0,\mathbf{R}}^\dagger t_{-1,\mathbf{R}}$. One could then rewrite the original Hamiltonian of Bose-Hubbard model in terms of such new field operators. The completeness of such truncated phase space is ensured by applying a constrain: $\sum_{\alpha=-1}^1 t_{\alpha,\mathbf{R}}^\dagger t_{\alpha,\mathbf{R}} = 1$. In order to apply a variational meanfield study (i.e. Gutzwiller-type ground state), we make a unitary transform to a coherent state basis: $\vec{t}_{\mathbf{R}} = \mathcal{U} \cdot \vec{b}_{\mathbf{R}}$, where $\vec{t}_{\mathbf{R}} \equiv [t_{0,\mathbf{R}}^\dagger, t_{1,\mathbf{R}}^\dagger, t_{-1,\mathbf{R}}^\dagger]^T$ and $\vec{b}_{\mathbf{R}} \equiv [b_{0,\mathbf{R}}^\dagger, b_{1,\mathbf{R}}^\dagger, b_{2,\mathbf{R}}^\dagger]^T$. The transform matrix, \mathcal{U} , depends on some variational parameters (see Ref. [16] and Appendix B), which are determined by minimizing the variational energy, $\langle \Psi_{MF} | H | \Psi_{MF} \rangle$, with $|\Psi_{MF}\rangle \equiv \prod_{\mathbf{R}} b_{0,\mathbf{R}}^\dagger |0\rangle$ being the trial wavefunction at $T = 0$. Such meanfield calculation can give a meanfield quantum phase boundary between SF phase and MI phase, as shown in Fig. 1(b). The tip position in (b) can be found to be at $U_c = zJ(\sqrt{n_0 + 1} + \sqrt{n_0})^2$, and $\mu_c = (n_0 - \frac{1}{2})U - \frac{zJ}{2}$ (here $z = 6$ is the number of nearest neighboring sites in a 3D square lattice). Fixing the average density to be an integer, n_0 , the chemical potential at $T = 0$ changes as a function of U as the dashed line of Fig. 1(b). Defining $\delta\mu = \mu - (n_0 - \frac{1}{2})U$ as the chemical potential deviation from the middle of MI lobe at $U = \infty$, such particle-hole symmetric (i.e. integer filling) line can be obtained to be: $\delta\mu = -\frac{1}{4}[zJ + U(\sqrt{n_0 + 1} + \sqrt{n_0})^{-2}]$ in the SF side and $\delta\mu = -zJ/2$ in the MI side. The finite temperature phase diagram in (a) is plotted along such integer filling line.

To calculate the quasi-particle excitation and the associated quantum depletion energy, Altman *et al.* [16] further used Holstein-Primakoff bosons to eliminate $b_{0,\mathbf{R}}$ and $b_{0,\mathbf{R}}^\dagger$ in order to obtain an effective Hamiltonian to the quadratic order of quasi-particles, $b_{1/2,\mathbf{R}}$. In the SF phase, the obtained effective Hamiltonian can be further diagonalized by using a canonical transformation in momentum space (i.e. a generalized Bogoliubov transformation), $\vec{b}_{\mathbf{k}} = \mathcal{M} \cdot \vec{\beta}_{\mathbf{k}}$, where $\vec{b}_{\mathbf{k}} \equiv [b_{1,\mathbf{k}}, b_{2,\mathbf{k}}, b_{1,\mathbf{k}}^\dagger, b_{2,\mathbf{k}}^\dagger]^T$ and $\vec{\beta}_{\mathbf{k}} \equiv [\beta_{s,\mathbf{k}}, \beta_{m,\mathbf{k}}, \beta_{s,\mathbf{k}}^\dagger, \beta_{m,\mathbf{k}}^\dagger]^T$ (see Appendix B). Here \mathcal{M} is the transformation matrix, and $\beta_{s/m,\mathbf{k}}$ are the quasi-particle field operators for the sound mode and the massive mode respectively. In the long wavelength limit, their dispersion becomes $\epsilon_s(\mathbf{k}) = v_s|\mathbf{k}|$ and $\epsilon_m(\mathbf{k}) = \Delta_m + \mathbf{k}^2/2m^*$, where v_s is sound velocity, Δ_m is the mass gap and m^* is the effective mass of the massive excitation. Using $\xi = (U_c - U)/J$ to measure the distance from the critical point, U_c , we find that for integer

filling (along the dashed line of Fig. 1(b)):

$$v_s = \frac{\pi\sqrt{n_0(1+n_0)\xi/z}}{(\sqrt{n_0+1} - \sqrt{n_0})^2} + \mathcal{O}(\xi^{3/2}) \quad (3)$$

$$\Delta_m = \frac{\sqrt{n_0(1+n_0)}(1+2n_0) - 2n_0(1+n_0)}{(\sqrt{n_0+1} - \sqrt{n_0})^4}\xi + \mathcal{O}(\xi^2) \quad (4)$$

near the critical point (i.e. $\xi \ll 1$). Similar to the ordinary Bogoliubov transformation in the single component case, the quantum depleted particles can be also derived from such canonical transformation, which is very significant when near the quantum critical point, U_c . We note that recent calculation [18] on the spectral weights of these excitations show that the massive excitation in the superfluid regime has a rather short life time compared to the low energy phonon excitations. This result, however, cannot be correctly captured within the three-state model used in our recent paper.

In the Mott state, the ground state can be described by the three-state model even better, due to the strong reduction of number fluctuations. Within the meanfield approximation, the MI ground state is still described by a product state with integer number of particle per site, $|\Psi_{MF}\rangle = \prod_{\mathbf{R}} t_{0,\mathbf{R}}^\dagger |0\rangle = \prod_{\mathbf{R}} b_{0,\mathbf{R}}^\dagger |0\rangle$. As a result, the obtained effective Hamiltonian can be easily diagonalized by another canonical transformation [16]:

$$\begin{aligned} t_{-1,\mathbf{k}} &= -B(\mathbf{k})\beta_{p,\mathbf{k}}^\dagger - A(\mathbf{k})\beta_{h,-\mathbf{k}} \\ t_{1,-\mathbf{k}}^\dagger &= A(\mathbf{k})\beta_{p,\mathbf{k}}^\dagger + B(\mathbf{k})\beta_{h,-\mathbf{k}}, \end{aligned} \quad (5)$$

where $\beta_{p/h,\mathbf{k}}$ is the field operators for particle/hole excitation. Here $A(\mathbf{k}) \equiv \cosh(D_{\mathbf{k}}/2)$ and $B(\mathbf{k}) \equiv \sinh(D_{\mathbf{k}}/2)$ are coefficients with

$$\tanh(D_{\mathbf{k}}) \equiv \frac{-2\epsilon_0(\mathbf{k})\sqrt{n_0(n_0+1)}}{U - \epsilon_0(\mathbf{k})(2n_0+1)}, \quad (6)$$

and $\epsilon_0(\mathbf{k}) = 2J \sum_{\alpha=1}^d \cos(k_\alpha a)$. The particle and hole excitation dispersion are given by

$$\epsilon_{p(h)}(\mathbf{k}) = \mp [\epsilon_0(\mathbf{k})/2 + \delta\mu] + \tilde{\omega}(\mathbf{k}), \quad (7)$$

where $\delta\mu$ is the chemical potential measured from $(n_0 - \frac{1}{2})U$, $\epsilon_0(\mathbf{k}) = 2J \sum_{\alpha=1}^3 \cos(k_\alpha)$, and

$$\tilde{\omega}(\mathbf{k}) = \frac{1}{2}\sqrt{U^2 - U\epsilon_0(\mathbf{k})(4n_0+2) + \epsilon_0(\mathbf{k})^2}. \quad (8)$$

At zero temperature, the particle and hole excitations have gaps:

$$\Delta \equiv \epsilon_p(0) + \epsilon_h(0) = \sqrt{U^2 - zUJ(4n_0+2) + (zJ)^2}. \quad (9)$$

Near the critical point, we have $\Delta = 2(n_0(n_0 + 1))^{1/4}\sqrt{zJ\delta U} + \mathcal{O}(U^{3/2})$ with $\delta U \equiv U - U_c$. In the strong interacting limit, we have $\Delta = U + 2zJ\sqrt{n_0(n_0+1)} + \mathcal{O}(U^{-1})$. In finite temperature, the chemical potential

($\delta\mu(T)$) is given by fixing the number of particles to be n_0 , i.e. number of particles are the same as number of holes: $\frac{1}{\Omega} \sum_{\mathbf{k}} [f_B(\epsilon_{p,\mathbf{k}}) - f_B(\epsilon_{h,\mathbf{k}})] = 0$. More details can be found in Appendix C.

Using the meanfield ground states and quasi-particle excitations described above, in the rest of this paper we will study the momentum distribution at finite temperature. Our results should be able to give a quantitative prediction for the study of SF-MI quantum phase transition in the experimentally relevant regime.

IV. MOMENTUM DISTRIBUTION IN THE WEAKLY INTERACTING SUPERFLUID PHASE

We first study the momentum distribution in the weakly interacting regime by using the Bogoliubov-Hartree-Fock-Popov approximation [17]. We could separate the calculation in two different regimes of temperature: (i) $T > T_c$, (2) $T < T_c$. They correspond to regions, N1, and SF1 respectively in Fig. 1(a). In the normal state regime, it has been shown [17] that the self-energy shift to the single particle dispersion is just a constant, $\epsilon_{\mathbf{k}} = \epsilon_{b,\mathbf{k}} + 2n_0U$, where $\epsilon_{b,\mathbf{k}} = 2zJ - \epsilon_0(\mathbf{k})$ is the single particle band energy measured from the bottom ($\mathbf{k} = 0$) and n_0 is the average filling fraction. As a result, the chemical potential is also shifted by a constant and the transition temperature, T_c , is the same as the noninteracting system, giving by (set $k_B \equiv 1$) $n_0 = \frac{1}{\Omega} \sum_{\mathbf{k}} (e^{\epsilon_b(\mathbf{k})/T_c} - 1)^{-1}$. For a 3D square lattice, we have $T_c/J = 5.86$ for $n_0 = 1$ and $T_c/J = 10.29$ for $n_0 = 2$. When T is very close to T_c from above, the momentum distribution can be well approximated to be a Lorentzian function: $n^{\text{N1}}(\mathbf{k}) \sim \frac{T/J}{(|\mathbf{k}|^2 + k_{\text{th}}^{\text{N1}2})a^2}$ in the long wavelength limit, where $k_{\text{th}}^{\text{N1}}a = \sqrt{|\mu(T) - 2n_0U|/J} = 1.073(\delta T/T_c)^{1/2}$ is the thermal wavevector and $\delta T \equiv T - T_c$. When $T \rightarrow T_c$, the thermal momentum $k_{\text{th}}^{\text{N1}} \ll \pi/a$, and therefore we could calculate $N_{\perp}(\mathbf{q}_{\perp})$ by integrating k_z from $-\infty$ to ∞ as shown in Eq. (2). We obtain $N_{\perp}^{\text{N1}}(\mathbf{q}_{\perp}) = \frac{\pi T/t}{\sqrt{|\mathbf{q}_{\perp}|^2 + k_{\text{th}}^{\text{N1}2}}} |w(\mathbf{q}_{\perp})|^2$, where $w(\mathbf{q}_{\perp}) \propto e^{-|\mathbf{q}_{\perp}|^2 \sigma^2}$ is a broad Gaussian function due to the small onsite Wannier function of width $\sigma < a$ within the single band approximation. As pointed out in Ref. [8], the TOF image obtained from $N_{\perp}^{\text{N1}}(\mathbf{q}_{\perp})$ can therefore have a ‘‘sharp peak’’ even when $T > T_c$. As a result, such TOF image can be easily mis-interpreted as the characteristic feature of condensation. This simple analysis shows the importance for an quantitative analysis for the TOF image in the optical lattice.

When the temperature is below T_c (i.e. region SF1 of Fig. 1(a)), we can treat $a_0^{\dagger} = a_0$ as a c -number (i.e. condensate at $\mathbf{k} = 0$) and apply the Bogoliubov-Hartree-Fock-Popov approximation to diagonalize the quadratic order of the resulting effective Hamiltonian. Following the standard approach [17], we can obtain the phonon dispersion: $\epsilon_B(\mathbf{k}) = \sqrt{\epsilon_b(\mathbf{k})(\epsilon_b(\mathbf{k}) + 2n_0U_0)}$, and the

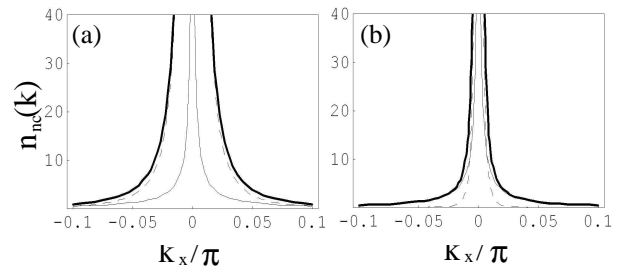


FIG. 3: Momentum distribution of non-condensate particles for (a) $T/J = 0.2$ and (b) $T/J = 0.02$ in region SF1 of Fig. 1(a). Thin solid and dashed lines are $n_{\text{qn}}^{\text{SF1}}(\mathbf{k})$ and $n_{\text{th}}^{\text{SF1}}(\mathbf{k})$ respectively, and thick solid lines are their sum. Here we use $U/J = 0.5$, $n_0 = 1$ and $k_y = k_z = 0$. Approximated results of Eq. (10) cannot be distinguished with the total distribution (thick line).

momentum distribution can be divided into two parts: $n^{\text{SF1}}(\mathbf{k}) = n_{\text{con}}^{\text{SF1}}\delta(\mathbf{k}) + n_{\text{nc}}^{\text{SF1}}(\mathbf{k})$, where $n_{\text{con}}^{\text{SF1}}$ is the number density of condensate particles and $n_{\text{nc}}^{\text{SF1}}(\mathbf{k}) = n_{\text{th}}^{\text{SF1}}(\mathbf{k}) + n_{\text{qn}}^{\text{SF1}}(\mathbf{k})$ is the momentum distribution of non-condensate particles. Here $n_{\text{th}}^{\text{SF1}}(\mathbf{k}) = \frac{\epsilon_b(\mathbf{k}) + n_0U_0}{\epsilon_B(\mathbf{k})} f_B(\epsilon_B(\mathbf{k}))$ and $n_{\text{qn}}^{\text{SF1}}(\mathbf{k}) = \frac{\epsilon_b(\mathbf{k}) + n_0U_0}{2\epsilon_B(\mathbf{k})} - \frac{1}{2}$ are the contribution from thermal excitation and quantum depletion respectively. $f_B(x) \equiv (e^{x/T} - 1)^{-1}$ is Bose-Einstein distribution function. Since the condensate part is a structure-less delta function in momentum space, here we concentrate on the momentum distribution of non-condensate particles. In Fig. 3, we show typical results of $n_{\text{th}}^{\text{SF1}}(\mathbf{k})$ and $n_{\text{qn}}^{\text{SF1}}(\mathbf{k})$ for comparison. We note that, even *without* adding the Wannier function, $n_{\text{th}}^{\text{SF1}}(\mathbf{k})$ and $n_{\text{qn}}^{\text{SF1}}(\mathbf{k})$ can have different shape in both long and short wavelength limit: as shown in Fig. 3(b), $n_{\text{nc}}^{\text{SF1}}(\mathbf{k})$ is dominated by thermal excitation in the long wavelength limit, while dominated by quantum depletion in the large momentum regime. This feature also makes it easy to be mis-interpreted as a ‘‘bimodal structure’’ of condensate, although we do not include the condensate particles yet. This situation will become more serious and crucial when near the quantum critical point, where the number of condensate particles can be small while the ‘‘bimodal structure’’ still exists due to the different momentum distribution of thermal and quantum excitation.

To further study the underlying physics in this regime, we note that there are two momentum scales involved in above expression: one is thermal momentum, $k_{\text{th}}^{\text{SF1}}a \equiv \sqrt{T/J}$ and the other is quantum momentum, $k_{\text{qn}}^{\text{SF1}}a \equiv \sqrt{n_0U/2J}$. There are three regimes we need to identify: (i) In weak interaction limit, we have $k_{\text{qn}}^{\text{SF1}} \ll k_{\text{th}}^{\text{SF1}}$ and hence the most relevant momentum regime is $k_{\text{qn}}^{\text{SF1}} \ll |\mathbf{k}| \ll k_{\text{th}}^{\text{SF1}}$, dominated by the thermal excitation. As a result, using $\epsilon_B(\mathbf{k}) \sim \epsilon_b(\mathbf{k})$ for $|\mathbf{k}| > k_{\text{qn}}^{\text{SF1}}$, we find $n_{\text{nc}}^{\text{SF1}}(\mathbf{k}) \sim n_{\text{th}}^{\text{SF1a}}(\mathbf{k}) \sim \frac{k_{\text{th}}^{\text{SF1}2}}{|\mathbf{k}|^2}$ in this region. (ii) In extremely low temperature region, we have $k_{\text{th}}^{\text{SF1}} \ll k_{\text{qn}}^{\text{SF1}}$, and the most relevant momentum regime becomes

$k_{\text{th}}^{\text{SF1}} \ll |\mathbf{k}| \ll k_{\text{qn}}^{\text{SF1}}$, dominated by the quantum depletion instead. Neglecting the thermal contribution in this region, we find $n_{\text{nc}}^{\text{SF1}}(\mathbf{k}) \sim n_{\text{qn}}^{\text{SF1}}(\mathbf{k}) \sim \frac{k_{\text{qn}}^{\text{SF1}2}}{4|\mathbf{k}|}$ (iii) In the intermediate regime ($U \sim T$), we have $k_{\text{th}}^{\text{SF1}} \sim k_{\text{qn}}^{\text{SF1}}$ and the most relevant momentum regime is from $|\mathbf{k}| < k_{\text{th}}^{\text{SF1}}, k_{\text{qn}}^{\text{SF1}}$. The the leading contribution of non-condensate particles can be obtained by expanding in the long wavelength limit:

$$\begin{aligned} n_{\text{nc}}^{\text{SF1}}(\mathbf{k}) &\sim \frac{(k_{\text{th}}^{\text{SF1}}a)^2}{2|\mathbf{k}|^2a^2} + c_0 - c_2|\mathbf{k}|^2a^2 \\ &\sim \frac{(k_{\text{th}}^{\text{SF1}}a)^2}{2|\mathbf{k}|^2a^2} + \frac{c_0}{1 + (c_2/c_0)|\mathbf{k}|^2a^2}, \end{aligned} \quad (10)$$

where

$$c_0 = \frac{(k_{\text{th}}^{\text{SF1}}a)^2}{24} + \frac{1}{8} \frac{(k_{\text{th}}^{\text{SF1}})^2}{(k_{\text{qn}}^{\text{SF1}})^2} + \frac{1}{6} \frac{(k_{\text{qn}}^{\text{SF1}})^2}{(k_{\text{th}}^{\text{SF1}})^2} - \frac{1}{2} \quad (11)$$

and

$$c_2 = \frac{1}{32} \frac{(k_{\text{th}}^{\text{SF1}})^2}{(k_{\text{qn}}^{\text{SF1}})^4} + \frac{1}{90} \frac{(k_{\text{qn}}^{\text{SF1}})^4}{(k_{\text{th}}^{\text{SF1}})^6} - \frac{(k_{\text{th}}^{\text{SF1}})^2}{480} - \frac{1}{12(k_{\text{th}}^{\text{SF1}}a)^2}. \quad (12)$$

Our numerical calculation shows that Eq. (10) is a very good approximation for the full Bogoliubov result ($< 1\%$) for $T/J > 0.1$ and $n_0U/J < 10$, covering most superfluid regime that current experiment can access. After column integration over k_z (we can extend the integration range to $(-\infty, \infty)$ if only $k_{\text{th}/\text{qn}}^{\text{SF1}} \ll \pi$), we find

$$N_{\perp}^{\text{SF1}}(\mathbf{q}_{\perp}) \sim \left(\frac{(k_{\text{th}}^{\text{SF1}})^2}{4|\mathbf{q}_{\perp}|} + \frac{c_0^2/2}{\sqrt{c_2(c_0 + c_2|\mathbf{q}_{\perp}|^2)}} \right) |w(\mathbf{q}_{\perp})|^2 \quad (13)$$

in this regime. Eq. (13) can be used to fit the experimental data to obtain the temperature and average filling fraction inside the optical lattice (We note that the overall amplitude is arbitrary and therefore only two parameters in Eq. (13) are needed). In above analysis, we did not discuss the structure of condensate part, which is supposed to be a sharp peak at $\mathbf{q} = 0$ with width π/L . The details of the condensate shape may be strongly affected by the interaction effect in the beginning of expansion. On the other hand, our analysis on the non-condensate particles above provides a quantitative and analytic equation for experimentalists to study the thermal/quantum tails for $\mathbf{q}_{\perp} \neq 0$. These parts is much less affected by interaction during the expansion and therefore can be a much more reliable method to extract the temperature inside optical lattice.

V. MOMENTUM DISTRIBUTION IN THE STRONGLY INTERACTING SUPERFLUID PHASE NEAR SF-MI TRANSITION POINT

When the interaction U is large enough, the quantum depletion of the condensate particles becomes significant,

and therefore the Bogoliubov approach cannot be justified, especially when close to the SF-MI transition point. More precisely, for the case of unit filling, $n_0 = 1$, the Bogoliubov approach used above is justified when $U \ll J$ (i.e. $k_{\text{qn}}^{\text{SF1}}a = \sqrt{n_0U/2J} \ll 1$), while the SF-MI transition occurs at $U \sim J$. In the later regime, the number fluctuation at each lattice size is strongly reduced and the phase fluctuation becomes enhanced. In this regime, we can apply the three-state model to study the SF phase as briefly described in Section III. To calculate the momentum distribution in the optical lattice, $\langle a_{\mathbf{k}}^{\dagger} a_{\mathbf{k}} \rangle$, we need to apply a series of transformation to diagonalize the quantum fluctuation on top of the meanfield result of the three-state model. Details of the calculation is shown in Appendix B. Here we just shown the final result of the noncondensate part: $n_{\text{nc}}^{\text{SF2}}(\mathbf{k}) = n_{\text{th}}^{\text{SF2}}(\mathbf{k}) + n_{\text{qn}}^{\text{SF2}}(\mathbf{k})$, where the thermal ($n_{\text{th}}^{\text{SF2}}(\mathbf{k})$) and the quantum depleted ($n_{\text{qn}}^{\text{SF2}}(\mathbf{k})$) parts are respectively (see Eq. (B13)):

$$\begin{aligned} n_{\text{th}}^{\text{SF2}}(\mathbf{k}) &= (S_{11}(\mathbf{k})^2 + S_{33}(\mathbf{k})^2)f(\epsilon_{s,\mathbf{k}}) \\ &\quad + (S_{22}(\mathbf{k})^2 + S_{44}(\mathbf{k})^2)f(\epsilon_{m,\mathbf{k}}) \end{aligned} \quad (14)$$

$$n_{\text{qn}}^{\text{SF2}}(\mathbf{k}) = S_{33}(\mathbf{k})^2 + S_{44}(\mathbf{k})^2, \quad (15)$$

where $S_{ij}(\mathbf{k})$ is the matrix element of a 4×4 matrix defined in Eq. (B12). The TOF image, $N_{\perp}(\mathbf{q}_{\perp})$, can be also calculated directly from Eq. (2) based on above result. Unfortunately, the analytic expression for the momentum distribution is too complicated to be expressed even in the long wavelength limit. Therefore in this section we will just show the numerical results in various parameter regime.

Before showing the numerical result of momentum distribution, it is instructive to mention that above result can be used to calculate the interaction effect of the SF transition temperature, $T_c(U)$, (as shown in Fig. 1(a)), by requiring the conservation of total number of particles:

$$\frac{1}{\Omega} \sum_{\mathbf{k}} n_{\text{nc}}^{\text{SF2}}(\mathbf{k}) = n_0. \quad (16)$$

In other words, when $T < T_c$, the difference between the total number of particles and the non-condensate particles can be interpreted as the condensate particles, providing the superfluidity of the system. When the interaction is stronger and/or the temperature is larger, the condensate density becomes smaller so that the non-condensate particles, contributed both from the thermal excitation and the quantum depletion, becomes dominant. Although we just consider the quantum fluctuation to the quadratic order within the three-state model, the obtained transition temperature (shown in Fig. 1(a)) is qualitatively consistent with the general picture, decreasing dramatically near the SF-MI transition point at $T = 0$.

When the temperature is above T_c , the three-state model is still justified if only the temperature is much smaller than the on-site interaction U (i.e. small number fluctuation). Although the disappearance of the order

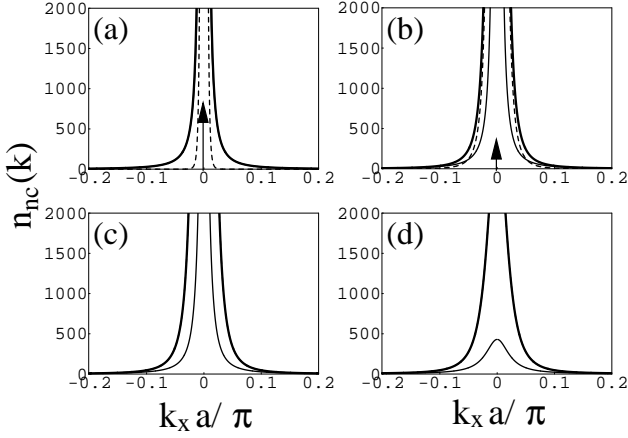


FIG. 4: Momentum distribution of non-condensate particles in 3D optical lattice with $U = 34J$ and $n_0 = 1$ for different temperature: $T/J = 0.1, 1, 1.5,$ and 1.7 respectively for (a)-(d). The solid and dashed lines are quantum depletion and thermal particles, and the thick solid lines are the total. Here $T_c = 1.2J$ and the upward arrows in (a) and (b) indicate the presence of condensate particles at $\mathbf{k} = 0$.

parameter (or condensation) makes the meanfield approach of the three-state model not well-justified, but quadratic expansion of the elementary excitation (i.e. $b_{1/2, \mathbf{R}}$) in the effective Hamiltonian can be still a good approximation if the number fluctuation is still small due to the strong interaction in the low temperature regime (i.e. $U \gg T > T_c$). As a result, we can still calculate the momentum distribution above T_c by tuning the chemical potential away from the value inside the superfluid phase, in order to conserve the total number of particles. In fact, such deviation of the chemical potential above T_c automatically leads to the disappearance of the Goldstone mode and then renormalizes the effective mass of the quasi-particle excitation.

In Fig. 4 we show the numerical results of the momentum distribution in the optical lattice for the thermal and quantum depleted particles in this regime. Different from the results of weakly interacting regime (SF1), the quantum depletion can still dominate the momentum distribution of non-condensate particle near the critical point, U_c , at low temperature regime (Fig. 4(a)). When the temperature is approaching T_c from below, however, the thermal excited particles become dominant in the momentum distribution (Fig. 4(b)). Similar to the situation of weakly interacting regime discuss above, momentum distribution of both quantum depleted and thermal excited particles are divergent in the long wavelength limit for $T < T_c$, making the distinguishment between condensate particles and non-condensate particles highly non-trivial, at least in a uniform system. When the temperature is above T_c , the contribution of condensate particles disappears and the momentum distribution becomes a Gaussian-like function with the width increased as a function of temperature.

VI. MOMENTUM DISTRIBUTION IN MOTT INSULATOR PHASE

Now we move to the study of finite temperature momentum distribution in the Mott insulator regime (in regions N4, and N5 of Fig. 1(a)), where the particle number fluctuation at each lattice site is strongly reduced. As mentioned in Section III, in the three-state model [16] the quasi-particle excitation can be calculated analytically, leading to a powerful tool to study the momentum distribution analytically. After some straightforward but tedious calculation (details are in Appendix C), the full momentum distribution can be also contributed from thermal part and quantum depletion part as before: $n_{\text{nc}}^{\text{MI}}(\mathbf{k}) = n_{\text{th}}^{\text{MI}}(\mathbf{k}) + n_{\text{qn}}^{\text{MI}}(\mathbf{k})$, where

$$n_{\text{th}}^{\text{MI}}(\mathbf{k}) = -\delta n + f_B(\epsilon_{p, \mathbf{k}}) (\sqrt{n_0 + 1}A(\mathbf{k}) - \sqrt{n_0}B(\mathbf{k}))^2 + f_B(\epsilon_{h, \mathbf{k}}) (\sqrt{n_0 + 1}B(\mathbf{k}) - \sqrt{n_0}A(\mathbf{k}))^2, \quad (17)$$

$$n_{\text{qn}}^{\text{MI}}(\mathbf{k}) = (\sqrt{n_0 + 1}B(\mathbf{k}) - \sqrt{n_0}A(\mathbf{k}))^2 \quad (18)$$

as shown in Eq. (C24). Here $A(\mathbf{k})$ and $B(\mathbf{k})$ have been defined in Eqs. (5) and (6) above. δn a constant density shift due to thermal excitation, and can be calculated from Eq. (C7) (see more details in Appendix C).

Since the single particle tunneling, J , is much smaller than onsite interaction, U , in this regime, there are only two temperature limit we need to consider: (i) in the low temperature regime ($U \gg T, J$, i.e. region N4 of Fig. 1(a)), and (ii) in the high temperature regime ($T \sim U \gg J$, i.e. region N5 of Fig. 1(a)). From the calculation shown in Appendix C, in the low temperature region ($U \gg T, J$), the chemical potential can be calculated to be (see Eq. (C15)): $e^{\delta\mu/T} = \left(\frac{I_0\left(\frac{2n_0J}{T}\right)}{I_0\left(\frac{2(n_0+1)J}{T}\right)} \right)^{3/2}$, where $I_0(x)$ is the modified Bessel function. As a result, we find the momentum distribution of quantum depleted particles and the thermal excited particles can be calculated explicitly to the leading order of J/U and T/U (see Eq. (C24)):

$$n_{\text{qn}}^{\text{N4}}(\mathbf{k}) = n_0 + \frac{2n_0(1+n_0)}{U} \epsilon_0(\mathbf{k}), \quad (19)$$

$$n_{\text{th}}^{\text{N4}}(\mathbf{k}) = g_1 e^{(n_0+1)\epsilon_0(\mathbf{k})/T} + g_2 e^{n_0\epsilon_0(\mathbf{k})/T} - \delta n, \quad (20)$$

where $g_1 \equiv (1+n_0)e^{-U/2T}e^{\delta\mu/T}$ and $g_2 = n_0e^{-U/2T}e^{-\delta\mu/T}$ are small constants in this low temperature limit. $\delta n = (2n_0 + 1)e^{-U/2T}I_0\left(\frac{2n_0J}{T}\right)^{3/2}I_0\left(\frac{2(n_0+1)J}{T}\right)^{3/2}$ is a constant density shift due to thermal excitation as shown in Eq. (C7). The TOF image, $N_{\perp}(\mathbf{q}_{\perp})$, can be also calculated analytically in the leading order of large U to be (see

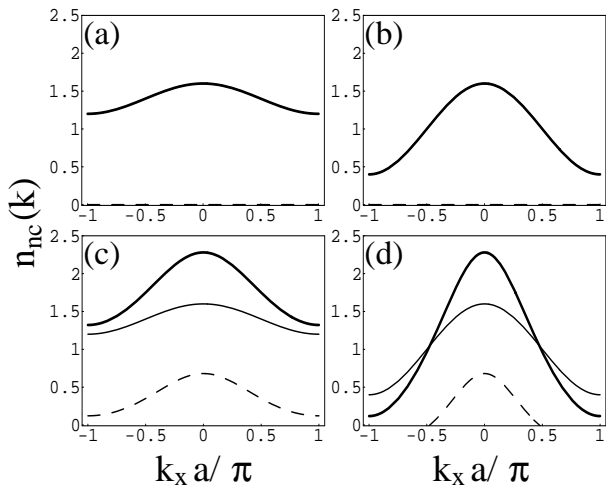


FIG. 5: Momentum distribution of non-condensate particles in the MI regime. (a) and (b) are for $T/J = 1$, and (c) and (d) are for $T/J = 10$. The left panels are distribution along k_x axis with $k_y = k_z = 0$, while the right panels are distribution along the diagonal direction, i.e. $\mathbf{k} = k(1, 1, 1)$. Thin dashed and thin solid lines are the thermal and quantum contribution respectively, and the thick solid lines are the total distribution. Here we use $U/J = 40$, and other parameters are the same as Fig. 3. Note that the thermal contribution in (d) becomes negative in the large momentum regime due to the constant density shift, δn . The total distribution, of course, is always positive definite.

Eqs. (C25) and (C26):

$$N_{\perp}^{N4}(\mathbf{q}_{\perp}) = \left[n_0 + \frac{4n_0(1+n_0)J}{U}(\cos(q_x) + \cos(q_y)) - \delta n + G_1 e^{2J(n_0+1)(\cos(q_x)+\cos(q_y))/T} + G_2 e^{2Jn_0(\cos(q_x)+\cos(q_y))/T} \right] |w(\mathbf{q}_{\perp})|^2 \quad (21)$$

where $G_2 = g_1 I_0(\frac{2J(n_0+1)}{T})$ and $G_2 = g_2 I_0(\frac{2Jn_0}{T})$.

One interesting thing in the above close form expression is that the momentum distribution is different from the pure meanfield result ($N_{\perp}(\mathbf{q}_{\perp}) = n_0$) by additional contribution from both thermal fluctuation of quasi-particles and the quantum depletion. The thermal excited particles can contribute a very narrow peak when $T \ll J$, because $e^{n_0 \epsilon_0(q_x, 0)/T} \propto e^{2n_0 J \cos(q_x a)/T} \sim e^{2n_0 J/T(1-q_x^2 a^2/2)}$, showing a characteristic momentum scale, $\sqrt{T/n_0 J a^2}$, in the long wavelength limit. Although such narrow peak structure on top of a uniform momentum distribution looks surprising, but it is consistent with the sharpe peak structure of a normal state just above the superfluid T_c in the weakly interacting regime [8].

Now we consider the high temperature regime when $T \sim U \gg J$, as the region N5 in Fig. 1. In this regime, the chemical potential correction, $\delta\mu$, can be shown to be very small, to the second order of J/T : $\frac{\delta\mu}{T} = \frac{-3(2n_0+1)}{2} \coth(\frac{U}{4T}) (\frac{J}{T})^2$, as explicitly calculated in Eq. (C22). This result indicated that the chemical

potential, μ , is almost the same as the value at the middle of MI lobe in the large U limit even in the system of low filling fraction ($n_0 \sim 1$), reflecting the fact that the particle and hole excitations are almost the same (particle-hole symmetry) in this high temperature limit. As a result, to the leading order of small single particle tunneling, J , the momentum distribution can be calculated to be (see Eq. (C27) and Appendix C for details): $n_{nc}^{N5}(\mathbf{k}) = n_{th}^{N5}(\mathbf{k}) + n_{qn}^{N5}(\mathbf{k})$, where

$$n_{qn}^{N5}(\mathbf{k}) = n_0 + 2n_0(1+n_0) \frac{\epsilon_0(\mathbf{k})}{U} \quad (22)$$

$$n_{th}^{N5}(\mathbf{k}) = h_1 \frac{\epsilon_0(\mathbf{k})}{U} + h_2 \frac{\epsilon_0(\mathbf{k})}{T}. \quad (23)$$

Here we define the two constants, $h_1 = \frac{4n_0(1+n_0)}{e^{U/2T}-1}$, and $h_2 = \frac{(1+2n_0+2n_0^2)e^{U/2T}}{(e^{U/2T}-1)^2}$. Note that the contribution of δn is cancelled in the regime, see Eq. (C27). It is easy to see that in this regime, the thermal excitation contributes the same momentum distribution ($\propto \epsilon_0(\mathbf{k})$) as the one contributed by quantum depletion. This is very different from the result in the low temperature limit (see $n_{th}^{N4}(\mathbf{k})$ above). This is because, in the low temperature limit, the thermal wavelength can be very long, leading to a small momentum distribution of the thermal excited quasi-particles. However, when the temperature is increased, the thermal wavelength becomes shorter and even the same order as the lattice constant, and hence the momentum distribution is broad in momentum space. The TOF image obtained by integrating over the k_z component can be also calculated easily (see Eqs. (C28) and (C29)):

$$N_{\perp}(\mathbf{q}_{\perp}) = \left[n_0 + H_1 \frac{\epsilon_0(\mathbf{q}_{\perp})}{J} \right] |w(\mathbf{q}_{\perp})|^2 \quad (24)$$

where $H_1 = \frac{2n_0(1+n_0)J}{U} \left[1 + \frac{2}{e^{U/2T}-1} \right] + \frac{(1+2n_0+2n_0^2)e^{U/2T}}{(e^{U/2T}-1)^2} \frac{J}{T}$.

VII. MOMENTUM DISTRIBUTION AT QUANTUM CRITICAL POINT

When near the quantum phase transition point (say N3 of Fig. 1), the meanfield treatment becomes unjustified due to large fluctuations. However, we find that it is still possible to extract some useful information about the momentum distribution in the large n_0 limit, where the meanfield approximation becomes justified again, since the transition becomes more classical like. We can start from the analytic results in MI state by taking $U \rightarrow U_c$. Using the fact that $A(\mathbf{k}) = \cosh(D_{\mathbf{k}}/2)$ and $B(\mathbf{k}) = \sinh(D_{\mathbf{k}}/2)$ with $D_{\mathbf{k}}$ being defined in Eq.

(6), we find that in the large n_0 limit:

$$\begin{aligned} n_{\text{nc}}^{\text{MI}}(\mathbf{k}) &= f_B(\epsilon_{p,\mathbf{k}}) (\sqrt{n_0+1}A(\mathbf{k}) - \sqrt{n_0}B(\mathbf{k}))^2 - \delta n \\ &\quad + (1 + f_B(\epsilon_{h,\mathbf{k}})) (\sqrt{n_0+1}B(\mathbf{k}) - \sqrt{n_0}A(\mathbf{k}))^2 \\ &\sim n_0(1 + f_B(\epsilon_{p,\mathbf{k}}) + f_B(\epsilon_{h,\mathbf{k}}))(A(\mathbf{k}) - B(\mathbf{k}))^2. \end{aligned} \quad (25)$$

We also have

$$\begin{aligned} (A(\mathbf{k}) - B(\mathbf{k}))^2 &= e^{-D\mathbf{k}} \\ &\sim \sqrt{\frac{U - \epsilon_0(\mathbf{k})(2n_0 + 1 - 2\sqrt{n_0(n_0 + 1)})}{U - \epsilon_0(\mathbf{k})(2n_0 + 1 + 2\sqrt{n_0(n_0 + 1)})}} \\ &\sim \sqrt{1 - \frac{1}{u}\gamma_{\mathbf{k}}}, \end{aligned} \quad (26)$$

where $u \equiv U/4n_0zJ$ and $\gamma_{\mathbf{k}} \equiv z^{-1} \sum_{\delta} e^{i\mathbf{k}\cdot\delta}$ with δ being the direction to the nearest neighboring sites [16]. In other words, for 3D square lattice, $\epsilon_0(\mathbf{k}) \equiv J\gamma_{\mathbf{k}} = 2J \sum_{\alpha} \cos(k_{\alpha}a)$. Within the same approximation ($n_0 \gg 1$), we have $\epsilon_{p,\mathbf{k}} \sim \epsilon_{h,\mathbf{k}} = (U/2)\sqrt{1 - \gamma_{\mathbf{k}}/u}$, and therefore the momentum distribution becomes

$$\begin{aligned} n_{\mathbf{k}}^{\text{MI}} &\propto (1 + 2f_B(\epsilon_{p,\mathbf{k}})) \left(1 - \frac{1}{u}\gamma_{\mathbf{k}}\right)^{-1/2} \\ &\propto \coth\left(\frac{\epsilon_{p,\mathbf{k}} - \mu}{2k_B T}\right) \left(1 - \frac{1}{u}\gamma_{\mathbf{k}}\right)^{-1/2} \end{aligned} \quad (27)$$

This is the most general expression of finite temperature momentum distribution in the MI state in the large n_0 limit.

We find that above result can be also easily applied to the situation at critical point (N3 of Fig. 1), where $u = 1$ and $\mu = U/2$ in the large n_0 limit. In the long wavelength limit, we have $\gamma_{\mathbf{k}} \sim 1 - \frac{1}{6}a^2\mathbf{k}^2$, and therefore

$$n_{\mathbf{k}}^{\text{N3}} \propto \coth\left(\frac{U}{8k_B T}\right) \frac{1}{|\mathbf{k}|a} \quad (28)$$

upto some overall density shift, δn . When temperature is lowered, the amplitude becomes larger and hence the sharp peak is more pronounced. Note that in the low filling factor limit, $n_0 \sim 1$, the exact cancellation in above derivation will not exist, and therefore the momentum distribution function will be still finite at $\mathbf{k} = 0$, leading to a very sharp Lorentzian type distribution with a large correlation length.

VIII. EFFECTIVE THEORY AND THE SCALING LAW OF THE MOMENTUM DISTRIBUTION NEAR THE CRITICAL POINT

The quantum critical theory for the momentum distribution near the SF-MI quantum critical point at integer filling is belong to the universality class of the $d+1$ dimensional XY model [22] (here d is spatial dimensionality). Before performing a full calculation, several remarks

have to be mentioned: (i) It is known that the superfluid phase has only two independent fluctuations and therefore we can use XY model or quantum rotor model with degree of freedom $N = 2$ to investigate the quantum critical phenomena near the SF-MI transition. (ii) Since the *anomalous dimension*, η , is known to be just 0.03 for $D = 2$ dimension and has a small logarithmic correction for 3D system [23], we can expect that this problem can be very well approximated by the large N result, which is equivalent to the meanfield approximation in the limit of large filling fraction ($n \gg 1$). (iii) It is well-known that for 2D XY model, there is a classical Kosterlitz-Thouless transition, which has a power-law decay of the correlation function in low temperature limit. The quantum critical phenomena of such quasi-long-ranged order is highly non-trivial and therefore will not be included in our following analysis.

Based on above assumptions, we can consider the quantum field theory for large N limit and use the value of saddle point to write down the meanfield order parameters. Following the notation in Ref. [23], the resulting fluctuations of action above such meanfield state can be written as the following XY model (or say the quantum rotor model of $N = 2$ degree of freedom):

$$S = \frac{N}{2\tilde{c}\tilde{g}} \sum_{\alpha} \int d\mathbf{r} \int_0^{1/T} d\tau [(\partial_{\tau}n_{\alpha})^2 + \tilde{c}^2(\nabla n_{\alpha})^2 + \tilde{m}^2 n_{\alpha}^2] \quad (29)$$

where n_{α} for $\alpha = 1, 2$ is the component of quantum fluctuations. (The original Hubbard model has $U(1)$ symmetry, so that a complex order parameter with two independent components of quantum fluctuations are expected.) Here \tilde{c} is the renormalized phonon velocity, \tilde{g} is the renormalized interaction, and \tilde{m} is the renormalized mass term, which changes sign at the SF-MI phase transition boundary [22,23]. Note that the actual values of \tilde{g} , \tilde{c} and \tilde{m} have to be calculated from a microscopic theory after integrating over the high energy modes and therefore can be different from the meanfield results as we derived above within various regimes. However, since we are more interested in the universal form of momentum distribution rather than the quantitative values in this section, we will just keep them as a fitting parameters that might be able to be measured from the experimental data. Besides, in this paper we are interested in the results in the low energy (or long wavelength) limit, and therefore we can neglect the lattice potential

Here we first investigate the momentum distribution function in the normal state, which is a paramagnetic state in the spin (i.e. quantum rotor model with $N = 2$) language. Using the notation in Ref. [23], in the large N theory, the correlation function between different components of the quantum rotor is given by the following

fomula:

$$C_{\alpha\beta}(\mathbf{r}, \tau) \equiv \langle n_{\alpha}(\mathbf{r}, \tau) n_{\beta}(0, 0) \rangle \quad (30)$$

$$\begin{aligned} \chi_{\alpha\beta}(k, \omega_n) &\equiv \int_0^{1/T} d\tau \int d\mathbf{r} C_{\alpha\beta}(\mathbf{r}, \tau) e^{-i\mathbf{k}\cdot\mathbf{r} + i\omega_n\tau} \\ &= \chi(k, \omega_n) \delta_{\alpha,\beta} \end{aligned} \quad (31)$$

$$\chi(k, \omega) = \frac{\tilde{c}\tilde{g}/N}{\tilde{c}^2 k^2 - (\omega + i\delta)^2 + \tilde{m}^2}, \quad (32)$$

which is the single particle spectral function, and has been assumed to be isotropic in the low momentum regime (i.e. when the fluctuation length scale is much larger than lattice constant). As a result, the susceptibility χ above depends only on the value of momentum, $k = |\mathbf{k}|$. $\omega_n = 2\pi nT$ is the Matsubara frequencies, and we have let k_B and \hbar to be unit. In the last line of Eq. (31), we have used the fact that the correlation function of a paramagnetic state (i.e. normal state) should have the diagonal part only in the spin component.

The momentum distribution, $n(k)$, is obtained from the equal time correlation and therefore

$$\begin{aligned} n(k) &= T \sum_{\omega_n} \chi(k, \omega_n) \\ &= T \sum_{\omega_n} \frac{\tilde{c}\tilde{g}/N}{\tilde{c}^2 k^2 + \omega_n^2 + \tilde{m}^2}. \end{aligned} \quad (33)$$

Note that different behaviors of $n(k)$ in the different places of the phase diagram (Fig. 1(a)) just related to how the summation is calculated and how the mass term, m , changes in different regime near the critical point. Using the following identity: $\sum_{n=-\infty}^{\infty} \frac{1}{x^2 + n^2} = (\pi/x) \coth(x\pi)$, we can evaluate the spectral function and obtain:

$$n(k) = \frac{\tilde{c}\tilde{g}/2N}{\sqrt{\tilde{c}^2 k^2 + \tilde{m}^2}} \coth\left(\frac{\sqrt{\tilde{c}^2 k^2 + \tilde{m}^2}}{2T}\right). \quad (34)$$

When considering large T limit and finite mass term ($\tilde{m} \neq 0$), we use $\coth(x) \sim 1/x$ as $x \rightarrow 0$, we find

$$n(k) = \frac{\tilde{c}\tilde{g}T/N}{\tilde{c}^2 k^2 + \tilde{m}^2} = \frac{\tilde{c}\tilde{g}T/\tilde{m}N}{1 + \xi_c^2 k^2}, \quad (35)$$

which is the Lorentzian function one usually discussed in high temperature regime. $\xi_c = \tilde{c}/\tilde{m}$ is the coherent length. However, if we are looking at low temperature and/or large momentum regime, Eq. (34) gives

$$n(k) \sim \frac{\tilde{c}\tilde{g}/2N}{\sqrt{\tilde{c}^2 k^2 + \tilde{m}^2}} \sim k^{-1} \quad (36)$$

as $k \gg \tilde{m}/\tilde{c} = \xi_c^{-1}$. This result implies the different momentum dependence can be obtained when the momentum is larger or smaller than the inverse of correlation length, which is the length scale indicating the coherence of the entire system. If ξ_c is large (i.e. lower temperature and near the SF transition), most of the momentum

distribution will be dominated by the quantum fluctuations, $\propto k^{-1}$. On the other hand, if ξ_c is small (i.e. away from the SF transition), the most momentum distribution will be dominated by thermal fluctuations, which gives a Lorentzian type distribution.

Finally, if we consider the momentum distribution along the the phase transition boundary or inside the ordered phase at finite temperature, i.e. $\tilde{m} = 0$, we can find that at finite T :

$$\begin{aligned} n(k) &= \frac{\tilde{g}/2N}{|k|} \coth\left(\frac{\tilde{c}|k|}{2T}\right) \\ &\sim \begin{cases} \frac{\tilde{g}T}{Nc k^2} & T \gg \tilde{c}k \\ \frac{\tilde{g}}{2N|k|} & T \ll ck \end{cases} \end{aligned} \quad (37)$$

This shows two different behavior for large T (or small k) and small T (or large k regime). This result agree with our statement from the three state model that thermal fluctuation is dominant and diverges as k^{-2} in the small momentum regime, while the quantum fluctuation is dominant and scales as $|k|^{-1}$ in the large momentum regime.

IX. EXPERIMENTAL IMPLICATION

The TOF image is known to be the most important measurement in the systems of ultracold atoms. The long time of flight image is usually believed to be equivalent to the momentum distribution of the system inside the optical lattice. Our results show that how the different scaling behavior and temperature/interaction dependence of such distribution of non-condensate particle can be distinguished and identified. This is of particular importance when near the quantum critical point of the SF-MI transition. From experimental point of view, there are several methods to observe these different behaviors in the current experimental setup.

First of all, one can systematically investigate the TOF image for different initial temperature, and compare their TOF image both in the small and large momentum regime. According to our results, one should find that the TOF in the large momentum regime has little temperature dependence since it is mostly contributed by quantum fluctuations. On the other hand, after extract out the temperature dependent part of the TOF, one can use our analytical form of the thermal excitation (Eqs. (10) and (13)) to obtain the temperature and condensate density inside the optical lattice.

In recent experiments in Stanford's group [7], the TOF image of a condensate confined in the 1D optical lattice has been fitted and investigated by using three Gaussian-type function: one for condensate, one for thermal atoms, and one for quantum depletion. Although the system setup and parameter regimes in their experiment are different from the regimes we discuss in this paper, the clear

evidence for different temperature behaviors in the non-condensate particles still qualitatively supports our prediction: the quantum depleted particles dominates the large momentum distribution, while the thermal particles dominates the small momentum regime. Further investigation on the TOF image can be very interesting and useful for the future development.

Secondly, one can also separate the contribution of the thermal excitations from the quantum depletion by providing a potential gradient just before releasing the optical lattice. It is found [24] that due to the different linear response of these two non-condensate particles, the center of thermal particle distribution can be away from the quantum depleted particles, making the direct measurement of these two distribution functions available. This approach opens the possibility to quantitatively study the condensate and non-condensate profile near the quantum critical point.

X. SUMMARY

In this paper, we have explicitly shown that the momentum distribution of the quantum depleted non-condensate particles can be very different from the thermal excited noncondensate particles, especially when near the quantum critical point of SF-MI phase transition. Our results is also consistent with the general scaling properties derived from $N = 2$ quantum rotor model (i.e. XY model). Our analytical results can be used to provide a unique method to determine the temperature and condensate fraction inside the optical lattice. Further extension to the study of noise correlation function and/or other physical properties can be also expected in the same frame work.

XI. ACKNOWLEDGEMENT

The author appreciate the fruitful discussion with T.-L. Ho, T. Porto, I. Spielman, S. D. Huber, S. Sachdev and E. Demler. This work was initiated by the discussion with T.-L. Ho during the visit in Ohio State University. This work is supported by NSC Taiwan.

APPENDIX A: MOMENTUM DISTRIBUTION IN AN OPTICAL LATTICE AND IN FREE SPACE

1. Definition of wavefunction and their Fourier transform

We first identify the following four kinds of single particle wavefunctions in the optical lattice and clarify their relationship with each other. (i) $\Psi_{\mathbf{k}}(\mathbf{r})$ is the Bloch wavefunction in real space at a lattice quantum number, \mathbf{k} , in the first Brillouin Zone (BZ). (ii) $\tilde{\Psi}_{\mathbf{k}}(\mathbf{q})$ is its Fourier transform with respect to the real space coordinate, \mathbf{r} .

(iii) $w_{\mathbf{R}}(\mathbf{r})$ is the Wannier function, centered at a given lattice position, \mathbf{R} . $w_{\mathbf{R}}(\mathbf{r})$ is a Fourier transform of $\Psi_{\mathbf{k}}(\mathbf{r})$ with respect to the lattice momentum, \mathbf{k} . (iv) Finally, $\tilde{w}_{\mathbf{R}}(\mathbf{q})$ is the Fourier transform of $w_{\mathbf{R}}(\mathbf{r})$ with respect to the real space coordinate, \mathbf{r} . Their relationship are given as following (L is the number of total lattice point along each direction and a is the lattice constant. $\sum_{\mathbf{k}}'$ means a summation over the first BZ):

$$\tilde{\Psi}_{\mathbf{k}}(\mathbf{q}) = \int d\mathbf{r} e^{-i\mathbf{q}\cdot\mathbf{r}} \Psi_{\mathbf{k}}(\mathbf{r}) \quad (\text{A1})$$

$$\Psi_{\mathbf{k}}(\mathbf{r}) = \int \frac{d\mathbf{q}}{(2\pi)^3} e^{i\mathbf{q}\cdot\mathbf{r}} \tilde{\Psi}_{\mathbf{k}}(\mathbf{q}) \quad (\text{A2})$$

$$w_{\mathbf{R}}(\mathbf{r}) = \frac{1}{L^{3/2}} \sum_{\mathbf{k}}' e^{-i\mathbf{k}\cdot\mathbf{R}} \Psi_{\mathbf{k}}(\mathbf{r}) \quad (\text{A3})$$

$$\Psi_{\mathbf{k}}(\mathbf{r}) = \frac{1}{L^{3/2}} \sum_{\mathbf{R}} e^{i\mathbf{k}\cdot\mathbf{R}} w_{\mathbf{R}}(\mathbf{r}) \quad (\text{A4})$$

$$\tilde{w}_{\mathbf{R}}(\mathbf{q}) = \int d\mathbf{r} e^{-i\mathbf{q}\cdot\mathbf{r}} w_{\mathbf{R}}(\mathbf{r}) \quad (\text{A5})$$

$$w_{\mathbf{R}}(\mathbf{r}) = \int \frac{d\mathbf{q}}{(2\pi)^3} e^{i\mathbf{q}\cdot\mathbf{r}} \tilde{w}_{\mathbf{R}}(\mathbf{q}) \quad (\text{A6})$$

$$\tilde{w}_{\mathbf{R}}(\mathbf{q}) = \frac{1}{L^{3/2}} \sum_{\mathbf{k}}' e^{-i\mathbf{k}\cdot\mathbf{R}} \tilde{\Psi}_{\mathbf{k}}(\mathbf{q}) \quad (\text{A7})$$

$$\tilde{\Psi}_{\mathbf{k}}(\mathbf{q}) = \frac{1}{L^{3/2}} \sum_{\mathbf{R}} e^{i\mathbf{k}\cdot\mathbf{R}} \tilde{w}_{\mathbf{R}}(\mathbf{q}) \quad (\text{A8})$$

Note that the Fourier and the inverse Fourier transform convention is different for real space momentum and lattice momentum. The amplitude of a wavefunction can be shown to be normalized:

$$\begin{aligned} 1 &= \int d\mathbf{r} |\Psi_{\mathbf{k}}(\mathbf{r})|^2 = \int \frac{d\mathbf{q}}{(2\pi)^3} |\tilde{\Psi}_{\mathbf{k}}(\mathbf{q})|^2 \\ &= \int d\mathbf{r} |w_{\mathbf{R}}(\mathbf{r})|^2 = \int \frac{d\mathbf{q}}{(2\pi)^3} |\tilde{w}_{\mathbf{R}}(\mathbf{q})|^2 \end{aligned} \quad (\text{A9})$$

2. Momentum distribution

Now we need to identify the field operators based on the following three different basis: (i) lattice site basis (\mathbf{R}) with Wannier function ($w_{\mathbf{R}}(\mathbf{r})$) as an eigenstate, (ii) Bloch momentum basis (\mathbf{k}) with Bloch wavefunction ($\Psi_{\mathbf{k}}(\mathbf{r})$) as an eigenstate, and (3) free space momentum basis (\mathbf{q}) with plane waves ($\frac{e^{i\mathbf{q}\cdot\mathbf{r}}}{\sqrt{V}}$, and V is the volume of the whole system of free space) as an eigenstate. Their fields operators are defined to be $a_{\mathbf{R}}$, $a_{\mathbf{k}}$ and $b_{\mathbf{q}}$, respectively, and they are related to the single particle field

operator, $\hat{\Psi}(\mathbf{r})$, to be

$$\begin{aligned}\hat{\Psi}(\mathbf{r}) &= \sum_{\mathbf{R}} a_{\mathbf{R}} w_{\mathbf{R}}(\mathbf{r}) \\ &= \sum_{\mathbf{k}} ' a_{\mathbf{k}} \Psi_{\mathbf{k}}(\mathbf{r}) \\ &= \sum_{\mathbf{q}} b_{\mathbf{q}} \frac{e^{i\mathbf{q}\cdot\mathbf{r}}}{\sqrt{V}}.\end{aligned}\quad (\text{A10})$$

Therefore, these field operators can be transformed with each other as following:

$$a_{\mathbf{k}} \equiv \frac{1}{L^{3/2}} \sum_{\mathbf{R}} a_{\mathbf{R}} e^{-i\mathbf{k}\cdot\mathbf{R}} \quad (\text{A11})$$

$$b_{\mathbf{q}} = \frac{1}{\sqrt{V}} \sum_{\mathbf{k}} a_{\mathbf{k}} \tilde{\Psi}_{\mathbf{k}}(\mathbf{q}). \quad (\text{A12})$$

As a result, the momentum distribution in real space ($N(\mathbf{q})$) can be connected to the momentum distribution in lattice ($n(\mathbf{k})$) by

$$\begin{aligned}N(\mathbf{q}) &\equiv \langle b_{\mathbf{q}}^\dagger b_{\mathbf{q}} \rangle \\ &= \frac{1}{V} \sum_{\mathbf{k}} ' n(\mathbf{k}) \left| \tilde{\Psi}_{\mathbf{k}}(\mathbf{q}) \right|^2,\end{aligned}\quad (\text{A13})$$

where we have used $\langle a_{\mathbf{k}}^\dagger a_{\mathbf{k}'} \rangle = n(\mathbf{k}) \delta_{\mathbf{k},\mathbf{k}'}$.

It is known that when the lattice strength is strong, we can approximate the Wannier function of the lowest subband by a Gaussian-type function:

$$w_{\mathbf{R}}(\mathbf{r}) \approx \frac{1}{\pi^{3/4} \sigma^{3/2}} e^{-\frac{1}{2} |\mathbf{r}-\mathbf{R}|^2 / \sigma^2} \quad (\text{A14})$$

where σ is the Gaussian width. Therefore, we have

$$\begin{aligned}|\tilde{\Psi}_{\mathbf{k}}(\mathbf{q})|^2 &= \left| \frac{1}{L^{3/2}} \sum_{\mathbf{R}} \tilde{w}_{\mathbf{R}}(\mathbf{q}) e^{i\mathbf{k}\cdot\mathbf{R}} \right|^2 \\ &= f(\mathbf{k}-\mathbf{q}) |w(\mathbf{q})|^2,\end{aligned}\quad (\text{A15})$$

where

$$\begin{aligned}f(\mathbf{q}) &\equiv \frac{(2\pi)^3}{L^3} \left| \sum_{\mathbf{R}} e^{i\mathbf{q}\cdot\mathbf{R}} \right|^2 \\ &= \frac{(2\pi)^3}{L^3} \prod_{\alpha} \left| \frac{\sin(Lq_{\alpha}a/2)}{\sin(q_{\alpha}a/2)} \right|^2\end{aligned}\quad (\text{A16})$$

$$|w(\mathbf{q})|^2 \equiv \frac{\sigma^3}{\pi^{3/2}} e^{-|\mathbf{q}|^2 \sigma^2} \quad (\text{A17})$$

In the limit of large system size ($L \rightarrow \infty$), $f(\mathbf{q})$ becomes a periodic function of delta-function peaks at each reciprocal lattice, $\mathbf{G}_{\mathbf{n}} = (2\pi\mathbf{n}/a)$, where $\mathbf{n} = (n_1, n_2, n_3)$ is a vector of integer numbers. Within such approximation, the momentum distribution in free space can have a simple relationship with the momentum distribution in the optical lattice:

$$N(\mathbf{q}) \propto \sum_{\mathbf{n}} \sum_{\mathbf{k}} ' [n(\mathbf{k}) |w(\mathbf{q})|^2 \delta(\mathbf{k}-\mathbf{q}-\mathbf{G}_{\mathbf{n}})] \quad (\text{A18})$$

However, such simplified result is not correct if the system of finite size, where $f(\mathbf{q})$ is not a delta function, but just a sharp function at $\mathbf{G}_{\mathbf{n}}$.

3. Momentum distribution after column integration

The TOF image taking after a long expansion time can be understood as the momentum distribution after column integration along a certain direction (say z axis). Therefore, it is instructive to study the momentum distribution in free space after column integration along the z axis. From a general result of Eqs. (A15)-(A17), we have

$$\begin{aligned}N_{\perp}(\mathbf{q}_{\perp}) &= \frac{1}{V} \sum_{\mathbf{k}} ' n(\mathbf{k}) \int \frac{dq_z}{2\pi} \left| \tilde{\Psi}_{\mathbf{k}}(\mathbf{q}) \right|^2 \\ &= \frac{1}{V} \sum_{\mathbf{k}} ' n(\mathbf{k}) \frac{(2\pi)^3}{L^3} \frac{\sigma^3}{\pi^{3/2}} \\ &\quad \times \int \frac{dq_z}{2\pi} \sum_{\mathbf{R},\mathbf{R}'} e^{i(\mathbf{k}-\mathbf{q})\cdot(\mathbf{R}-\mathbf{R}')-\mathbf{q}^2\sigma^2} \\ &\propto \frac{1}{V} \sum_{\mathbf{k}} ' n(\mathbf{k}) \left| \tilde{\Psi}_{\mathbf{k}_{\perp}}(\mathbf{q}_{\perp}) \right|^2 \\ &\quad \times \sum_{R_z, R'_z} e^{ik_z(R_z-R'_z)} e^{-(R_z-R'_z)^2/4\sigma^2}\end{aligned}\quad (\text{A19})$$

where $\tilde{\Psi}_{\mathbf{k}_{\perp}}(\mathbf{q}_{\perp})$ is the Fourier transform of the 2D Bloch function in 2D lattice, similar to the 3D case defined in Eqs. (A1), (A15), (A16), and (A17).

To evaluate the summation over R_z and R'_z , we note that the first order cotribution comes from the case $R_z = R'_z$, while the second order contribution comes from $|R_z - R'_z| = a$, which is exponentially smaller the first order as $a \gg \sigma$ near the SF-MI transition regime. As a result, it will be a good approximation to keep the leading order contribution only and hence the momentum distribution in free space after column integration becomes

$$\begin{aligned}N_{\perp}(\mathbf{q}_{\perp}) &\propto \sum_{\mathbf{k}_{\perp}} ' n_{\perp}(\mathbf{k}_{\perp}) \left| \tilde{\Psi}_{\mathbf{k}_{\perp}}(\mathbf{q}_{\perp}) \right|^2 \\ &\propto n_{\perp}(\mathbf{k}_{\perp}) |w(\mathbf{q}_{\perp})|^2,\end{aligned}\quad (\text{A20})$$

if we are interested in the long wavelength limit ($\mathbf{q} \sim 0$) and approximate the function $f(\mathbf{q}_{\perp}) \propto \delta(\mathbf{q}_{\perp}-\mathbf{k}_{\perp})$ in the limit of infinite number of lattice ($L \rightarrow \infty$). Here

$$n_{\perp}(\mathbf{k}) \equiv \frac{1}{L} \sum_{k_z} ' n(\mathbf{k}) \quad (\text{A21})$$

is the momentum distribution in optical lattice after column integration.

APPENDIX B: FINITE TEMPERATURE MOMENTUM DISTRIBUTION IN SUPERFLUID PHASE

1. Canonical transformation

In order to clarify the complicated process, here we list all the transformation of quasi-particles used in the SF phase within the three-state model. Within the three-state model, Altman *et al.* [16] introduced a new operator, $t_{\alpha,\mathbf{R}}^\dagger|0\rangle \equiv \frac{1}{\sqrt{(n_0+\alpha)!}} (a_{\mathbf{R}}^\dagger)^{n_0+\alpha}|0\rangle = |n_0 + \alpha\rangle_{\mathbf{R}}$ to create a state of $n_0 + \alpha$ particles ($\alpha = \pm 1$ and 0) at site \mathbf{R} . As a result, one can show that within this truncated space, any local operator, say the bosonic field operator $a_{\mathbf{R}}$, and the particle number operator, $a_{\mathbf{R}}^\dagger a_{\mathbf{R}}$, can be respectively expressed to be

$$a_{\mathbf{R}} = \sqrt{n_0 + 1} t_{0,\mathbf{R}}^\dagger t_{1,\mathbf{R}} + \sqrt{n_0} t_{-1,\mathbf{R}}^\dagger t_{0,\mathbf{R}} \quad (\text{B1})$$

$$\begin{aligned} a_{\mathbf{R}}^\dagger a_{\mathbf{R}} &= (n_0 + 1) t_{1,\mathbf{R}}^\dagger t_{1,\mathbf{R}} + n_0 t_{0,\mathbf{R}}^\dagger t_{0,\mathbf{R}} \\ &\quad + (n_0 - 1) t_{-1,\mathbf{R}}^\dagger t_{-1,\mathbf{R}}. \end{aligned} \quad (\text{B2})$$

We note that in the three-state presentation, the number operator, $a_{\mathbf{R}}^\dagger a_{\mathbf{R}}$, is not a simple product of the result for $a_{\mathbf{R}}$ and $a_{\mathbf{R}}^\dagger$. This can be easily understood from the fact that when applying $a_{\mathbf{R}}^\dagger a_{\mathbf{R}}$ on a state $|n_0 - 1\rangle_{\mathbf{R}}$, the particle number can be virtually reduced to $n_0 - 2$ by $a_{\mathbf{R}}$ first then becomes its original value by $a_{\mathbf{R}}^\dagger$. such virtual process is not included in the three-state representation of $a_{\mathbf{R}}$. Such trivial notational problem occurs only in the situation when two or more field operators applying on the same lattice site.

Within the meanfield approximation, we can assume that the SF ground state is a coherent state composed by different number of states at each site, i.e. $|\Psi_{\text{MF}}\rangle \equiv \prod_{\mathbf{R}} b_{0,\mathbf{R}}^\dagger |0\rangle$, where $b_{0,\mathbf{R}}^\dagger = \cos(\theta/2) t_{0,\mathbf{R}}^\dagger + \sin(\theta/2)(\cos \chi t_{1,\mathbf{R}}^\dagger + \sin \chi t_{-1,\mathbf{R}}^\dagger)$ where θ and χ are two variational parameters [16]. When considering the quasi-particle excitation, Altman *et al.* further generalize above transformation to the following:

$$\begin{aligned} \begin{bmatrix} t_{0,\mathbf{R}}^\dagger \\ t_{1,\mathbf{R}}^\dagger \\ t_{-1,\mathbf{R}}^\dagger \end{bmatrix} &= \begin{bmatrix} \cos(\theta/2) & -\sin(\theta/2) & 0 \\ \sin(\theta/2) \cos \chi & \cos(\theta/2) \cos \chi & -\sin \chi \\ \sin(\theta/2) \sin \chi & \cos(\theta/2) \sin \chi & \cos \chi \end{bmatrix} \begin{bmatrix} b_{0,\mathbf{R}}^\dagger \\ b_{1,\mathbf{R}}^\dagger \\ b_{2,\mathbf{R}}^\dagger \end{bmatrix} \\ &\equiv \begin{bmatrix} U_{00} & U_{01} & U_{02} \\ U_{10} & U_{11} & U_{12} \\ U_{20} & U_{21} & U_{22} \end{bmatrix} \begin{bmatrix} b_{0,\mathbf{R}}^\dagger \\ b_{1,\mathbf{R}}^\dagger \\ b_{2,\mathbf{R}}^\dagger \end{bmatrix} \equiv \mathcal{U} \cdot \vec{b}_{\mathbf{R}}, \end{aligned} \quad (\text{B3})$$

where \mathcal{U} is the transform matrix, and $\vec{b}_{\mathbf{R}} \equiv [b_{0,\mathbf{R}}^\dagger, b_{1,\mathbf{R}}^\dagger, b_{2,\mathbf{R}}^\dagger]^T$ is the vector of operators with $b_{1/2,\mathbf{R}}$ being the field operators for the excitations above the condensate state, $b_{0,\mathbf{R}}^\dagger$.

When in the SF state, one can approximate the sin-

gle particle ground state as a c -number, and apply the generalized bogoliubov transformation to diagonalize the system Hamiltonian upto the quadratic order of excitations. Such generalized Bogoliubov transformation can be written to be [16]

$$\vec{b}_{\mathbf{k}} \equiv \begin{bmatrix} b_{1,\mathbf{k}} \\ b_{2,\mathbf{k}} \\ b_{1,-\mathbf{k}}^\dagger \\ b_{2,-\mathbf{k}}^\dagger \end{bmatrix} = \begin{bmatrix} N_{11}(\mathbf{k}) & N_{12}(\mathbf{k}) & P_{11}(\mathbf{k}) & P_{12}(\mathbf{k}) \\ N_{12}(\mathbf{k}) & N_{22}(\mathbf{k}) & P_{12}(\mathbf{k}) & P_{22}(\mathbf{k}) \\ P_{11}(-\mathbf{k}) & P_{12}(-\mathbf{k}) & N_{11}(-\mathbf{k}) & N_{12}(-\mathbf{k}) \\ P_{12}(-\mathbf{k}) & P_{22}(-\mathbf{k}) & N_{12}(-\mathbf{k}) & N_{22}(-\mathbf{k}) \end{bmatrix} \begin{bmatrix} \beta_{s,\mathbf{k}} \\ \beta_{m,\mathbf{k}} \\ \beta_{s,-\mathbf{k}}^\dagger \\ \beta_{m,-\mathbf{k}}^\dagger \end{bmatrix} \equiv \mathcal{M} \cdot \vec{\beta}_{\mathbf{k}} \quad (\text{B4})$$

where the definition of the excited states, $\vec{b}_{\mathbf{k}}$ and $\vec{\beta}_{\mathbf{k}}$ are clearly shown as above. $\mathcal{M}(\mathbf{k})$ is the 4×4 transform matrix, which in principle can be derived analytically. However, since the full analytic expression is too complicated to be understood in a simple physical picture, here

we will use numerical method to evaluate them directly.

2. Momentum distribution of noncondensate particles

Our goal is to calculate the momentum distribution in optical lattice: $\langle a_{\mathbf{k}}^\dagger a_{\mathbf{k}} \rangle$, by using above transformations.

We first transform it into the t -operators:

$$\begin{aligned} \langle a_{\mathbf{k}}^\dagger a_{\mathbf{k}} \rangle &= \frac{1}{L^3} \sum_{\mathbf{R}, \mathbf{R}'} e^{i\mathbf{k} \cdot (\mathbf{R} - \mathbf{R}')} \left[(n_0 + 1) \langle t_{1, \mathbf{R}}^\dagger t_{0, \mathbf{R}} t_{0, \mathbf{R}'}^\dagger t_{1, \mathbf{R}'} \rangle + n_0 \langle t_{0, \mathbf{R}}^\dagger t_{-1, \mathbf{R}} t_{-1, \mathbf{R}'}^\dagger t_{0, \mathbf{R}'} \rangle \right. \\ &\quad \left. + \sqrt{n_0(n_0 + 1)} \left(\langle t_{1, \mathbf{R}}^\dagger t_{0, \mathbf{R}} t_{-1, \mathbf{R}'}^\dagger t_{0, \mathbf{R}'} \rangle + \langle t_{0, \mathbf{R}}^\dagger t_{-1, \mathbf{R}} t_{0, \mathbf{R}'}^\dagger t_{1, \mathbf{R}'} \rangle \right) \right] \end{aligned} \quad (\text{B5})$$

The first term, defined to be T_1 upto the prefactor, $n_0 + 1$, gives

$$\begin{aligned} \frac{1}{L^3} \sum_{\mathbf{R}, \mathbf{R}'} e^{i\mathbf{k} \cdot (\mathbf{R} - \mathbf{R}')} \langle t_{1, \mathbf{R}}^\dagger t_{0, \mathbf{R}} t_{0, \mathbf{R}'}^\dagger t_{1, \mathbf{R}'} \rangle &= L^3 \delta_{\mathbf{k}, 0} U_{10}^2 U_{00}^2 \\ &+ U_{10} U_{00} \delta_{\mathbf{k}, 0} \sum_{\mathbf{R}} \left[\langle (U_{01} b_{1, \mathbf{R}}^\dagger + U_{02} b_{2, \mathbf{R}}^\dagger) (U_{11} b_{1, \mathbf{R}} + U_{12} b_{2, \mathbf{R}}) \rangle + \langle (U_{11} b_{1, \mathbf{R}}^\dagger + U_{12} b_{2, \mathbf{R}}^\dagger) (U_{01} b_{1, \mathbf{R}} + U_{02} b_{2, \mathbf{R}}) \rangle \right] \\ &+ \frac{1}{L^3} \sum_{\mathbf{R}, \mathbf{R}'} e^{i\mathbf{k} \cdot (\mathbf{R} - \mathbf{R}')} \left[U_{10}^2 \langle (U_{01} b_{1, \mathbf{R}} + U_{02} b_{2, \mathbf{R}}) (U_{01} b_{1, \mathbf{R}'}^\dagger + U_{02} b_{2, \mathbf{R}'}^\dagger) \rangle + U_{00}^2 \langle (U_{11} b_{1, \mathbf{R}}^\dagger + U_{12} b_{2, \mathbf{R}}^\dagger) (U_{11} b_{1, \mathbf{R}'} + U_{12} b_{2, \mathbf{R}'} \rangle \right] \\ &+ \frac{U_{10} U_{00}}{L^3} \sum_{\mathbf{R}, \mathbf{R}'} e^{i\mathbf{k} \cdot (\mathbf{R} - \mathbf{R}')} \left[\langle (U_{01} b_{1, \mathbf{R}} + U_{02} b_{2, \mathbf{R}}) (U_{11} b_{1, \mathbf{R}'} + U_{12} b_{2, \mathbf{R}'} \rangle + \langle (U_{11} b_{1, \mathbf{R}}^\dagger + U_{12} b_{2, \mathbf{R}}^\dagger) (U_{01} b_{1, \mathbf{R}'}^\dagger + U_{02} b_{2, \mathbf{R}'}^\dagger) \rangle \right], \end{aligned} \quad (\text{B6})$$

where we have used the approximation: $b_{0, \mathbf{R}} \sim 1 - \frac{1}{2} b_{1, \mathbf{R}}^\dagger b_{1, \mathbf{R}} - \frac{1}{2} b_{2, \mathbf{R}}^\dagger b_{2, \mathbf{R}}$ to eliminate $b_{0, \mathbf{R}}$ to the quadratic order of small fluctuation, $b_{1/2, \mathbf{R}}$. The first two terms are proportional to the system size, L^3 , and are nonzero only at $\mathbf{k} = 0$, indicating a contribution from the condensate particles. The last two terms, however, are the noncondensate part. Since in our paper, we are interested in the momentum distribution at finite lattice momentum

\mathbf{k} , we will concentrate on the later part for the numerical calculation of momentum distribution.

Below we define the momentum distribution of the noncondensate particle from the i th term of Eq. (B5) to be T_i ($i = 1, 2, 3, 4$) (not including the prefactor, $n_0, n_0 + 1$, or $\sqrt{n_0(n_0 + 1)}$), and these terms can be expressed in the momentum space to be

$$T_1 = \left\langle \begin{bmatrix} b_{1, \mathbf{k}}^\dagger \\ b_{2, \mathbf{k}}^\dagger \\ b_{1, -\mathbf{k}} \\ b_{2, -\mathbf{k}} \end{bmatrix}^T \begin{bmatrix} U_{00}^2 U_{11}^2 & U_{00}^2 U_{11} U_{12} & U_{10} U_{00} U_{11} U_{01} & U_{10} U_{00} U_{11} U_{02} \\ U_{00}^2 U_{11} U_{12} & U_{00}^2 U_{12}^2 & U_{10} U_{00} U_{12} U_{01} & U_{10} U_{00} U_{12} U_{02} \\ U_{10} U_{00} U_{01} U_{11} & U_{10} U_{00} U_{01} U_{12} & U_{10}^2 U_{01}^2 & U_{10}^2 U_{01} U_{02} \\ U_{10} U_{00} U_{02} U_{11} & U_{10} U_{00} U_{02} U_{12} & U_{10}^2 U_{01} U_{02} & U_{10}^2 U_{02}^2 \end{bmatrix} \begin{bmatrix} b_{1, \mathbf{k}} \\ b_{2, \mathbf{k}} \\ b_{1, -\mathbf{k}}^\dagger \\ b_{2, -\mathbf{k}}^\dagger \end{bmatrix} \right\rangle \quad (\text{B7})$$

$$T_2 = \left\langle \begin{bmatrix} b_{1, \mathbf{k}}^\dagger \\ b_{2, \mathbf{k}}^\dagger \\ b_{1, -\mathbf{k}} \\ b_{2, -\mathbf{k}} \end{bmatrix}^T \begin{bmatrix} U_{20}^2 U_{01}^2 & U_{20}^2 U_{02} U_{01} & U_{20} U_{00} U_{01} U_{21} & U_{20} U_{00} U_{01} U_{22} \\ U_{20}^2 U_{02} U_{01} & U_{20}^2 U_{02}^2 & U_{20} U_{00} U_{02} U_{21} & U_{20} U_{00} U_{02} U_{22} \\ U_{20} U_{00} U_{21} U_{01} & U_{20} U_{00} U_{21} U_{02} & U_{10}^2 U_{21}^2 & U_{00}^2 U_{21} U_{22} \\ U_{20} U_{00} U_{22} U_{01} & U_{20} U_{00} U_{22} U_{02} & U_{00}^2 U_{21} U_{22} & U_{00}^2 U_{22}^2 \end{bmatrix} \begin{bmatrix} b_{1, \mathbf{k}} \\ b_{2, \mathbf{k}} \\ b_{1, -\mathbf{k}}^\dagger \\ b_{2, -\mathbf{k}}^\dagger \end{bmatrix} \right\rangle \quad (\text{B8})$$

$$T_3 = \left\langle \begin{bmatrix} b_{1, \mathbf{k}}^\dagger \\ b_{2, \mathbf{k}}^\dagger \\ b_{1, -\mathbf{k}} \\ b_{2, -\mathbf{k}} \end{bmatrix}^T \begin{bmatrix} U_{00} U_{20} U_{11} U_{01} & U_{00} U_{20} U_{11} U_{02} & U_{00}^2 U_{11} U_{21} & U_{00}^2 U_{11} U_{22} \\ U_{00} U_{20} U_{12} U_{01} & U_{00} U_{20} U_{12} U_{02} & U_{00}^2 U_{12} U_{21} & U_{00}^2 U_{12} U_{22} \\ U_{10} U_{20} U_{01}^2 & U_{10} U_{20} U_{02} U_{01} & U_{10} U_{00} U_{01} U_{21} & U_{10} U_{00} U_{01} U_{22} \\ U_{10} U_{20} U_{01} U_{02} & U_{10} U_{20} U_{02}^2 & U_{10} U_{00} U_{02} U_{21} & U_{10} U_{00} U_{02} U_{22} \end{bmatrix} \begin{bmatrix} b_{1, \mathbf{k}} \\ b_{2, \mathbf{k}} \\ b_{1, -\mathbf{k}}^\dagger \\ b_{2, -\mathbf{k}}^\dagger \end{bmatrix} \right\rangle, \quad (\text{B9})$$

$$(\text{B10})$$

and the forth term (T_4) is the exactly the complex conjugate of the third term (T_3). Therefore after including the proper prefactor in Eq. (B5), the total effect of non-condensate particle can be obtained by adding them together to be

$$\begin{aligned} \langle a_{\mathbf{k}}^\dagger a_{\mathbf{k}} \rangle_{\mathbf{k} \neq 0} &= (n_0 + 1)T_1(\mathbf{k}) + n_0 T_2(\mathbf{k}) \\ &\quad + \sqrt{n_0(n_0 + 1)}(T_3(\mathbf{k}) + T_4(\mathbf{k})) \\ &\equiv \vec{b}_{\mathbf{k}}^\dagger \cdot \mathcal{T}(\mathbf{k}) \cdot \vec{b}_{\mathbf{k}}, \end{aligned} \quad (\text{B11})$$

where $\vec{b}_{\mathbf{k}} \equiv [b_{1,\mathbf{k}}, b_{2,\mathbf{k}}, b_{1,-\mathbf{k}}^\dagger, b_{2,-\mathbf{k}}^\dagger]^T$ and $\mathcal{T}(\mathbf{k})$ is the result of the final 4×4 matrix (not the same as the 3×3 transform matrix, \mathcal{U} , defined in Eq. (B3)).

In the final step, we have to transform the operator of $b_{1/2,\pm\mathbf{k}}$ to $\beta_{s/m,\pm\mathbf{k}}$ (as shown in Eq. (B4)) to calculate the expectation value. The obtain momentum distribution from the noncondensate particles can therefore be written to be

$$\begin{aligned} \langle a_{\mathbf{k}}^\dagger a_{\mathbf{k}} \rangle_{\mathbf{k} \neq 0} &= \vec{b}_{\mathbf{k}}^\dagger \cdot \mathcal{T}(\mathbf{k}) \cdot \vec{b}_{\mathbf{k}} \\ &= \vec{\beta}_{\mathbf{k}}^\dagger \cdot \mathcal{M}(\mathbf{k})^\dagger \cdot \mathcal{T}(\mathbf{k}) \cdot \mathcal{M}(\mathbf{k}) \vec{\beta}_{\mathbf{k}} \\ &\equiv \vec{\beta}_{\mathbf{k}}^\dagger \cdot \mathcal{S}(\mathbf{k}) \cdot \vec{\beta}_{\mathbf{k}}, \end{aligned} \quad (\text{B12})$$

where the new matrix $\mathcal{S}(\mathbf{k}) \equiv \mathcal{M}(\mathbf{k})^\dagger \cdot \mathcal{T}(\mathbf{k}) \cdot \mathcal{M}(\mathbf{k})$. Using the fact that $\langle \beta_{s/m,\mathbf{k}}^\dagger \beta_{s/m,\mathbf{k}} \rangle = f_B(\epsilon_{s/m,\mathbf{k}})$ for the Bose-

Einstein distribution of particle/hole excitation. Therefore, the final result of the noncondensate particle momentum distribution can be expressed by the matrix elements of matrix $\mathcal{S}(\mathbf{k})$:

$$\begin{aligned} \langle a_{\mathbf{k}}^\dagger a_{\mathbf{k}} \rangle_{\mathbf{k} \neq 0} &= (S_{11}(\mathbf{k})^2 + S_{33}(\mathbf{k})^2) f(\epsilon_{s,\mathbf{k}}) \\ &\quad + (S_{22}(\mathbf{k})^2 + S_{44}(\mathbf{k})^2) f(\epsilon_{m,\mathbf{k}}) \\ &\quad + S_{33}(\mathbf{k})^2 + S_{44}(\mathbf{k})^2, \end{aligned} \quad (\text{B13})$$

where the last two terms are the contribution of quantum depleted particles.

APPENDIX C: FINITE TEMPERATURE MOMENTUM DISTRIBUTION IN MOTT INSULATOR PHASE

1. General expression in three-state model

In the Mott insulator phase, the meanfield ground state has one particle per site. Therefore it is important to separate the contribution of onsite density operator, $a_{\mathbf{R}}^\dagger a_{\mathbf{R}}$, from other non-local density operators. In order words, when calculating the momentum distribution, we have

$$\begin{aligned} \langle a_{\mathbf{k}}^\dagger a_{\mathbf{k}} \rangle &= \frac{1}{L^3} \sum_{\mathbf{R}_1, \mathbf{R}_2} a_{\mathbf{R}_1}^\dagger a_{\mathbf{R}_2} e^{i\mathbf{k} \cdot (\mathbf{R}_1 - \mathbf{R}_2)} = \frac{1}{L^3} \sum_{\mathbf{R}} \langle a_{\mathbf{R}}^\dagger a_{\mathbf{R}} \rangle + \frac{1}{L^3} \sum_{\mathbf{R}_1 \neq \mathbf{R}_2} \langle a_{\mathbf{R}_1}^\dagger a_{\mathbf{R}_2} \rangle e^{i\mathbf{k} \cdot (\mathbf{R}_1 - \mathbf{R}_2)} \\ &= \frac{1}{L^3} \sum_{\mathbf{R}} \langle [(n_0 + 1)t_{1,\mathbf{R}}^\dagger t_{1,\mathbf{R}} + n_0 t_{0,\mathbf{R}}^\dagger t_{0,\mathbf{R}} + (n_0 - 1)t_{-1,\mathbf{R}}^\dagger t_{-1,\mathbf{R}}] \rangle \\ &\quad - \frac{1}{L^3} \sum_{\mathbf{R}} \langle [\sqrt{n_0 + 1}t_{1,\mathbf{R}}^\dagger t_{0,\mathbf{R}} + \sqrt{n_0}t_{0,\mathbf{R}}^\dagger t_{-1,\mathbf{R}}] [\sqrt{n_0 + 1}t_{0,\mathbf{R}}^\dagger t_{1,\mathbf{R}} + \sqrt{n_0}t_{-1,\mathbf{R}}^\dagger t_{0,\mathbf{R}}] \rangle \\ &\quad + \frac{1}{L^3} \sum_{\mathbf{R}_1, \mathbf{R}_2} \langle [\sqrt{n_0 + 1}t_{1,\mathbf{R}_1}^\dagger t_{0,\mathbf{R}_1} + \sqrt{n_0}t_{0,\mathbf{R}_1}^\dagger t_{-1,\mathbf{R}_1}] [\sqrt{n_0 + 1}t_{0,\mathbf{R}_2}^\dagger t_{1,\mathbf{R}_2} + \sqrt{n_0}t_{-1,\mathbf{R}_2}^\dagger t_{0,\mathbf{R}_2}] \rangle e^{i\mathbf{k} \cdot (\mathbf{R}_1 - \mathbf{R}_2)}, \end{aligned} \quad (\text{C1})$$

where in the last line, for the convenience of later Fourier transform into momentum space, we have added the term of $\mathbf{R}_1 = \mathbf{R}_2$ and subtracted it in the second term.

Before transforming to the momentum space representation for the calculation of quasi-particle distribution, we can simplify above results further by using the num-

ber constrain, $\sum_{\alpha=-1}^1 t_{n_0+\alpha,\mathbf{R}}^\dagger t_{n_0+\alpha,\mathbf{R}} = 1$ to replace the field operator, $t_{0,\mathbf{R}}$ and $t_{0,\mathbf{R}}^\dagger$ to the quadratic order of small fluctuation. After some straightforward calculation, it is easy to show that

$$\begin{aligned} \langle a_{\mathbf{k}}^\dagger a_{\mathbf{k}} \rangle &= n_0 - \frac{1}{L^3} \sum_{\mathbf{k}} \left[(n_0 + 1) \langle t_{1,\mathbf{k}}^\dagger t_{1,\mathbf{k}} \rangle + n_0 \langle t_{-1,\mathbf{k}}^\dagger t_{-1,\mathbf{k}} \rangle + \sqrt{n_0(n_0 + 1)} \left(\langle t_{-1,-\mathbf{k}}^\dagger t_{1,\mathbf{k}} \rangle + \langle t_{1,\mathbf{k}}^\dagger t_{-1,-\mathbf{k}} \rangle \right) \right] \\ &\quad + (n_0 + 1) \langle t_{1,\mathbf{k}}^\dagger t_{1,\mathbf{k}} \rangle + n_0 \langle t_{-1,\mathbf{k}}^\dagger t_{-1,\mathbf{k}} \rangle + \sqrt{n_0(n_0 + 1)} \left[\langle t_{-1,-\mathbf{k}}^\dagger t_{1,\mathbf{k}} \rangle + \langle t_{1,\mathbf{k}}^\dagger t_{-1,-\mathbf{k}} \rangle \right], \end{aligned} \quad (\text{C2})$$

where in the last line we apply Fourier transform, $t_{\alpha,\mathbf{k}} = \frac{1}{L^{3/2}} \sum_{\mathbf{R}} t_{\alpha,\mathbf{R}} e^{-i\mathbf{k}\cdot\mathbf{R}}$, to the momentum space representation. Note that the first line of the last equation is independent of momentum \mathbf{k} , and therefore can be understood as a constant shift of the momentum distribution.

$$\langle t_{1,\mathbf{k}}^\dagger t_{1,\mathbf{k}} \rangle = A(\mathbf{k})^2 \langle \beta_{p,-\mathbf{k}}^\dagger \beta_{p,-\mathbf{k}} \rangle + B(\mathbf{k})^2 \langle \beta_{h,\mathbf{k}} \beta_{h,\mathbf{k}}^\dagger \rangle = A(\mathbf{k})^2 f_B(\epsilon_{p,\mathbf{k}}) + B(\mathbf{k})^2 (1 + f_B(\epsilon_{h,\mathbf{k}})), \quad (\text{C3})$$

$$\langle t_{-1,\mathbf{k}} t_{-1,\mathbf{k}}^\dagger \rangle = B(\mathbf{k})^2 f_B(\epsilon_{p,\mathbf{k}}) + A(\mathbf{k})^2 (1 + f_B(\epsilon_{h,\mathbf{k}})), \quad (\text{C4})$$

$$\langle t_{1,\mathbf{k}}^\dagger t_{-1,-\mathbf{k}}^\dagger \rangle = \langle t_{-1,-\mathbf{k}} t_{1,\mathbf{k}}^\dagger \rangle^* = -A(\mathbf{k})B(\mathbf{k})f_B(\epsilon_{p,\mathbf{k}}) - A(\mathbf{k})B(\mathbf{k})(1 + f_B(\epsilon_{h,\mathbf{k}})), \quad (\text{C5})$$

where $f_B(\epsilon_{p/h,\mathbf{k}}) = \langle \beta_{p/h,-\mathbf{k}}^\dagger \beta_{p/h,-\mathbf{k}} \rangle$ is the Bose-Einstein distribution of particle/hole excitations.

Therefore we can obtain the final expression of the momentum distribution, $n(\mathbf{k}) \equiv \langle a_{\mathbf{k}}^\dagger a_{\mathbf{k}} \rangle$, to be

$$n(\mathbf{k}) = -\delta n + f_B(\epsilon_{p,\mathbf{k}}) (\sqrt{n_0 + 1}A(\mathbf{k}) - \sqrt{n_0}B(\mathbf{k}))^2 + (1 + f_B(\epsilon_{h,\mathbf{k}})) (\sqrt{n_0 + 1}B(\mathbf{k}) - \sqrt{n_0}A(\mathbf{k}))^2, \quad (\text{C6})$$

where the density shift, δn is defined by

$$\delta n \equiv \frac{1}{L^3} \sum_{\mathbf{k}} \left[(\sqrt{n_0 + 1}A(\mathbf{k}) - \sqrt{n_0}B(\mathbf{k}))^2 f_B(\epsilon_{p,\mathbf{k}}) + (\sqrt{n_0 + 1}B(\mathbf{k}) - \sqrt{n_0}A(\mathbf{k}))^2 (1 + f_B(\epsilon_{h,\mathbf{k}})) \right] - n_0 \quad (\text{C7})$$

to ensure the conservation of total number of particles.

2. Analytical calculation of chemical potential

In order to evaluate the momentum distribution in the normal state regime, the first thing is to determine the chemical potential by fixing the total number of particles. We can use the general expression of momentum distribution, i.e. $\langle a_{\mathbf{R}}^\dagger a_{\mathbf{R}} \rangle$ in Eq. (C1), and obtain the total number of particles to be

$$\begin{aligned} N &= \sum_{\mathbf{k}} \langle a_{\mathbf{k}}^\dagger a_{\mathbf{k}} \rangle = \sum_{\mathbf{R}} \langle a_{\mathbf{R}}^\dagger a_{\mathbf{R}} \rangle \\ &= L^3 n_0 + \sum_{\mathbf{R}} \langle t_{1,\mathbf{R}}^\dagger t_{1,\mathbf{R}} - t_{-1,\mathbf{R}}^\dagger t_{-1,\mathbf{R}} \rangle \\ &= N + \sum_{\mathbf{k}} \langle t_{1,\mathbf{k}}^\dagger t_{1,\mathbf{k}} - t_{-1,\mathbf{k}}^\dagger t_{-1,\mathbf{k}} \rangle. \end{aligned} \quad (\text{C8})$$

Now if we transfer the t -operator to the quasi-particle operators, $\beta_{p/h,\mathbf{k}}$, in the MI state via Eq. (5), the conservation of total number of particle can be expressed to

We now calculate the expectation value for each term by transforming to the quasi-particle, $\beta_{\mathbf{k}}$, field via Eq. (5) and neglecting those particle non-conserving terms (for example, $\langle \beta_{p,\mathbf{k}} \beta_{p,\mathbf{k}} \rangle = \langle \beta_{h,\mathbf{k}}^\dagger \beta_{h,\mathbf{k}}^\dagger \rangle = \langle \beta_{p,\mathbf{k}}^\dagger \beta_{h,\mathbf{k}} \rangle = 0$). We have

be

$$\begin{aligned} 0 &= \sum_{\mathbf{k}} (A(\mathbf{k})^2 - B(\mathbf{k})^2) [f_B(\epsilon_{p,\mathbf{k}}) - f_B(\epsilon_{h,\mathbf{k}})] \\ &= \sum_{\mathbf{k}} [f_B(\epsilon_{p,\mathbf{k}}) - f_B(\epsilon_{h,\mathbf{k}})], \end{aligned} \quad (\text{C9})$$

which is nothing but the difference of particle excitations and hole excitations. Below we will investigate analytically the chemical potential in different parameter regimes of interest.

a. In the low temperature limit, $U \gg T, J$

We first consider the situation when $U \gg T, J$, so that we can use large U expansion for the particle and hole excitation spectrum and obtain

$$\begin{aligned} \epsilon_{p,\mathbf{k}} &= \frac{U}{2} - (\delta\mu + (n_0 + 1)\epsilon_0(\mathbf{k})) \\ &\quad - \frac{n_0(n_0 + 1)\epsilon_0(\mathbf{k})^2}{U} + \mathcal{O}((J/U)^2) \end{aligned} \quad (\text{C10})$$

$$\begin{aligned} \epsilon_{h,\mathbf{k}} &= \frac{U}{2} - (-\delta\mu + n_0\epsilon_0(\mathbf{k})) \\ &\quad - \frac{n_0(n_0 + 1)\epsilon_0(\mathbf{k})^2}{U} + \mathcal{O}((J/U)^2). \end{aligned} \quad (\text{C11})$$

Since $U \gg T$, we can expand the Bose-Einstein distribution function as

$$\begin{aligned} f_B(\epsilon(\mathbf{k})) &= \frac{1}{e^{\epsilon(\mathbf{k})/T} - 1} \\ &= \frac{1}{e^{(U/2 - \delta\epsilon(\mathbf{k}) \mp \delta\mu)/T} - 1} \\ &= e^{-(U/2 - \delta\epsilon(\mathbf{k}) \mp \delta\mu)/T} + \mathcal{O}(e^{-U/T}), \end{aligned} \quad (\text{C12})$$

where $\delta\epsilon(\mathbf{k}) \equiv (n_0 + 1)\epsilon_0(\mathbf{k})$ for particle excitation and $\delta\epsilon(\mathbf{k}) \equiv n_0\epsilon_0(\mathbf{k})$ for hole excitation. Now using the fact that $\int_{-\pi}^{\pi} \frac{dk}{2\pi} e^{x \cos(k)} = I_0(x)$, where $I_0(x)$ is the modified

Bessel function of the first kind, we can integrate out the momentum integral of Eq. (C9) and obtain

$$\frac{1}{L^3} \sum_{\mathbf{k}}' f_B(\epsilon_p(\mathbf{k})) = e^{-U/2T} e^{\delta\mu/T} \left[I_0 \left(\frac{2(n_0+1)J}{T} \right) \right]^3 \quad (\text{C13})$$

and

$$\frac{1}{L^3} \sum_{\mathbf{k}}' f_B(\epsilon_h(\mathbf{k})) = e^{-U/2T} e^{-\delta\mu/T} \left[I_0 \left(\frac{2n_0J}{T} \right) \right]^3 \quad (\text{C14})$$

Here we have neglected the higher order terms, which is proportional to $e^{-U/T} \ll 1$. As a result, the chemical potential can be calculated to be (from Eq. (C9))

$$e^{\delta\mu/T} = \left(\frac{I_0 \left(\frac{2n_0J}{T} \right)}{I_0 \left(\frac{2(n_0+1)J}{T} \right)} \right)^{3/2}, \quad (\text{C15})$$

which is good for all the temperature range if only $U \gg J, T$. If consider intermediate temperature regime, $U \gg T \gg J$, which is the most relevant regime in the present experiment, the leading order result gives

$$\frac{\delta\mu}{J} = -\frac{z}{4}(1+2n_0)\frac{J}{T} \quad (\text{C16})$$

where $z = 6$ in 3D and $z = 4$ for 2D systems.

On the other hand, in the limit of small T (i.e. $T \ll J$), we use $I_0(x) = \sqrt{\frac{\pi}{2x}} e^x$ and obtain

$$e^{\delta\mu/T} = \left(\frac{n_0+1}{n_0} \right)^{3/4} e^{-3J/T} \quad (\text{C17})$$

or

$$\delta\mu = -\frac{zJ}{2} + \frac{8T}{z} \log \left(\frac{n_0+1}{n_0} \right) \quad (\text{C18})$$

This is consistent with the results at $T = 0$.

b. In high temperature interaction limit, $T \sim U \gg J$

In the limit of high temperature, we can expand the excitation modes and Bose-einstein distribution to the leading order terms of small J/T and J/U . we have

$$\begin{aligned} \frac{1}{e^{\epsilon(\mathbf{k})/T} - 1} &= \frac{1}{e^{U/2T} e^{-(\delta\epsilon(\mathbf{k}) \pm \delta\mu)/T} - 1} = \frac{1}{e^{U/2T} - 1} + \frac{e^{U/2T}}{(e^{U/2T} - 1)^2} \frac{\delta\epsilon(\mathbf{k}) \pm \delta\mu}{T} \\ &+ \frac{1}{(e^{U/2T} - 1)^2} \left(\frac{e^{U/2T}}{e^{U/2T} - 1} - \frac{1}{2} e^{U/2T} \right) \left(\frac{\delta\epsilon(\mathbf{k}) \pm \delta\mu}{T} \right)^2 + \dots \end{aligned} \quad (\text{C19})$$

Therefore within the same order, the total number of particle and hole excitations shown in Eq. (C9) can be calculated to be (note that $\epsilon_0(\mathbf{k}) = 2J \sum_{\alpha} \cos(k_{\alpha}a)$ for 3D optical lattice.)

$$\frac{1}{\Omega} \sum_{\mathbf{k}}' f_B(\epsilon_p(\mathbf{k})) = \frac{1}{e^{U/2T} - 1} + \frac{e^{U/2T}}{(e^{U/2T} - 1)^2} \frac{\delta\mu}{T} + \frac{1}{(e^{U/2T} - 1)^2} \left(\frac{e^{U/2T}}{e^{U/2T} - 1} - \frac{1}{2} e^{U/2T} \right) \left(\frac{\delta\mu^2}{T^2} + z(n_0+1)\frac{J^2}{T^2} \right) \quad (\text{C20})$$

$$\frac{1}{\Omega} \sum_{\mathbf{k}}' f_B(\epsilon_h(\mathbf{k})) = \frac{1}{e^{U/2T} - 1} + \frac{e^{U/2T}}{(e^{U/2T} - 1)^2} \frac{-\delta\mu}{T} + \frac{1}{(e^{U/2T} - 1)^2} \left(\frac{e^{U/2T}}{e^{U/2T} - 1} - \frac{1}{2} e^{U/2T} \right) \left(\frac{\delta\mu^2}{T^2} + zn_0^2\frac{J^2}{T^2} \right). \quad (\text{C21})$$

The chemical potential then can be determined by the following colse form to the second order of J/T

$$\frac{\delta\mu}{T} = \frac{-z(2n_0+1)}{4} \coth \left(\frac{U}{4T} \right) \left(\frac{J}{T} \right)^2. \quad (\text{C22})$$

in the high temperature and strong interaction limit, $U \sim T \gg J$.

3. Analytical calculation of momentum distribution

a. In the low temperature limit, $U \gg T, J$

In order to study the momentum distribution shown in Eq. (C6), we can start from the following leading order expansion in the strong interaction limit ($U \gg T, J$) by using Eq. (6): $(\sqrt{n_0+1}B(\mathbf{k}) - \sqrt{n_0}A(\mathbf{k}))^2 \sim n_0$, and $(\sqrt{n_0+1}A(\mathbf{k}) - \sqrt{n_0}B(\mathbf{k}))^2 \sim 1 + n_0$. Now, after in-

cluding the large U expansion of particle-hole excitation shown in Eq. (C12), the density shift can be expressed to the leading order to be

$$\begin{aligned} \delta n &\equiv \frac{1}{L^3} \sum_{\mathbf{k}}' \left[(n_0 + 1) e^{-U/2T} e^{(n_0+1)\epsilon_0(\mathbf{k})/T} e^{\delta\mu/T} \right. \\ &\quad \left. + n_0 \left(1 + e^{-U/2T} e^{n_0\epsilon_0(\mathbf{k})/T} e^{-\delta\mu/T} \right) \right] - n_0 \\ &= (2n_0 + 1) e^{-U/2T} I_0 \left(\frac{2n_0 J}{T} \right)^{3/2} I_0 \left(\frac{2(n_0 + 1)J}{T} \right)^{3/2}. \end{aligned} \quad (\text{C23})$$

The momentum distribution then becomes

$$\begin{aligned} n(\mathbf{k}) &= (\sqrt{n_0 + 1} A(\mathbf{k}) - \sqrt{n_0} B(\mathbf{k}))^2 f_B(\epsilon_{p,\mathbf{k}}) + (\sqrt{n_0 + 1} B(\mathbf{k}) - \sqrt{n_0} A(\mathbf{k}))^2 (1 + f_B(\epsilon_{h,\mathbf{k}})) - \delta n \\ &= n_0 + 2n_0(1 + n_0) \frac{\epsilon_0(\mathbf{k})}{U} + (1 + n_0) \left(\frac{I_0(\frac{2n_0 J}{T})}{I_0(\frac{2(n_0+1)J}{T})} \right)^{3/2} e^{-U/2T} e^{(n_0+1)\epsilon_0(\mathbf{k})/T} \\ &\quad + n_0 \left(\frac{I_0(\frac{2(n_0+1)J}{T})}{I_0(\frac{2n_0 J}{T})} \right)^{3/2} e^{-U/2T} e^{n_0\epsilon_0(\mathbf{k})/T} - (2n_0 + 1) e^{-U/2T} I_0 \left(\frac{2n_0 J}{T} \right)^{3/2} I_0 \left(\frac{2(n_0 + 1)J}{T} \right)^{3/2}, \end{aligned} \quad (\text{C24})$$

to the leading order of large U , i.e. the next higher order is proportional to $(J/U) e^{-U/2T}$. It is easy to show that the total number of particles is conserved, i.e. $\frac{1}{L^3} \sum_{\mathbf{k}}' n(\mathbf{k}) = n_0$, and therefore above expression is a *close* form for the momentum distribution in large U limit. It is also straightforward to calculate the higher order terms but we will not show them here. From the momentum distribution in the optical lattice, we can also integrate out the z -component of the lattice momentum and obtain

$$\begin{aligned} n_{\perp}(\mathbf{k}_{\perp}) &= \frac{1}{L} \sum_{k_z} n(\mathbf{k}) \\ &= n_0 - \delta n + 2n_0(1 + n_0) \frac{\epsilon_0(\mathbf{k}_{\perp})}{U} \\ &\quad + G_1 e^{(n_0+1)\epsilon_0(\mathbf{k}_{\perp})/T} + G_2 e^{n_0\epsilon_0(\mathbf{k}_{\perp})/T}, \end{aligned} \quad (\text{C25})$$

where $\epsilon_0(\mathbf{k}_{\perp}) = 2J(\cos(k_x a) + \cos(k_y a))$ and

$$\begin{aligned} G_1 &= (1 + n_0) e^{-U/2T} \frac{I_0(\frac{2n_0 J}{T})^{3/2}}{I_0(\frac{2(n_0+1)J}{T})^{1/2}} \\ G_2 &= n_0 e^{-U/2T} \frac{I_0(\frac{2(n_0+1)J}{T})^{3/2}}{I_0(\frac{2n_0 J}{T})^{1/2}} \end{aligned} \quad (\text{C26})$$

b. High temperature limit, $T \sim U \gg J$

For the high temperature limit, we need to expand the whole formular in terms of J/T and J/U at the same time. To the leading order, we thus have

$$\begin{aligned} n(\mathbf{k}) &= (\sqrt{n_0 + 1} A(\mathbf{k}) - \sqrt{n_0} B(\mathbf{k}))^2 f_B(\epsilon_{p,\mathbf{k}}) + (\sqrt{n_0 + 1} B(\mathbf{k}) - \sqrt{n_0} A(\mathbf{k}))^2 (1 + f_B(\epsilon_{h,\mathbf{k}})) - \delta n \\ &\sim \left(1 + n_0 + 2n_0(1 + n_0) \frac{\epsilon_0(\mathbf{k})}{U} \right) \frac{1}{e^{U/2T} - 1} \left(1 + \frac{e^{U/2T}}{e^{U/2T} - 1} \frac{(n_0 + 1)\epsilon_0(\mathbf{k}) + \delta\mu}{T} \right) \\ &\quad + \left(n_0 + 2n_0(1 + n_0) \frac{\epsilon_0(\mathbf{k})}{U} \right) \left[1 + \frac{1}{e^{U/2T} - 1} \left(1 + \frac{e^{U/2T}}{e^{U/2T} - 1} \frac{n_0\epsilon_0(\mathbf{k}) - \delta\mu}{T} \right) \right] - \delta n \\ &\sim n_0 + 2n_0(1 + n_0) \frac{\epsilon_0(\mathbf{k})}{U} + \frac{4n_0(1 + n_0)}{e^{U/2T} - 1} \frac{\epsilon_0(\mathbf{k})}{U} + \frac{(1 + 2n_0 + 2n_0^2) e^{U/2T}}{(e^{U/2T} - 1)^2} \frac{\epsilon_0(\mathbf{k})}{T}, \end{aligned} \quad (\text{C27})$$

where the correction of chemical potential is the second order effect (Eq. (C22)) and has been neglected. In the

last line above, we also used the fact that δn is deter-

mined by requiring $\frac{1}{L^3} \sum_{\mathbf{k}} n(\mathbf{k}) = n_0$ to the leading order, and therefore obtained $\delta n = \frac{1+2n_0}{e^{U/2T}-1}$. Therefore, after integration over the k_z component, we have

$$n_{\perp}(\mathbf{k}_{\perp}) = n_0 + H_1 \epsilon_0(\mathbf{k}_{\perp})/J, \quad (\text{C28})$$

where

$$H_1 = \frac{2n_0(1+n_0)J}{U} \left[1 + \frac{2}{e^{U/2T}-1} \right] + \frac{(1+2n_0+2n_0^2)e^{U/2T}J}{(e^{U/2T}-1)^2} \frac{J}{T}. \quad (\text{C29})$$

- ¹ M. Greiner, *Nature* **415**, 39 (2002).
- ² F. Gerbier, *et al.*, *Phys. Rev. Lett.* **95**, 050404 (2005); I. B. Spielman, W. D. Phillips, and J. V. Porto, *Phys. Rev. Lett.* **98**, 080404 (2007); *ibid.* **100**, 120402 (2008); V. Guarrera, *et al.*, *Phys. Rev. Lett.* **100**, 250403 (2008); G. Roati, *et al.*, *Phys. Rev. Lett.* **99**, 010403 (2007).
- ³ For a review, please see, for example, I. Bloch, J. Dalinard, and W. Zwerger, *Rev. Mod. Phys.* **80**, 885 (2008).
- ⁴ The interaction effects during the TOF expansion was discussed shortly in Refs. [11,13] below. But a quantitative study has not been systematically investigated to the best of our knowledge.
- ⁵ K.W. Madison, F. Chevy, W. Wohlleben, and J. Dalibard, *Phys. Rev. Lett.* **84**, 806 (2000); J.R. Abo-Shaeer, C. Raman, J. M. Vogels, W. Ketterle, *Science* **292**, 476 (2001); M.R. Matthews, B.P. Anderson, P.C. Haljan, D.S. Hall, C.E. Wieman, and E.A. Cornell, *Phys. Rev. Lett.* **83**, 2498 (1999); D.E. Miller, Y. Liu, C. Stan, W. Setiawan, C. Sanner, K. Xu, W. Ketterle, and J.K. Chin, *Nature* **443**, 961 (2006).
- ⁶ K. Gunter, T. Stoferle, H. Moritz, M. Kohl, and T. Esslinger, *Phys. Rev. Lett.* **96**, 180402 (2006); S. Ospelkaus, C. Ospelkaus, O. Wille, M. Succo, P. Ernst, K. Sengstock, and K. Bongs, *Phys. Rev. Lett.* **96**, 180403 (2006).
- ⁷ Fitting with three Gaussian-type wavefunctions are also used in recent experiments of Stanford's group. Private communication.
- ⁸ R. B. Diener, Q. Zhou, H. Zhai, and T.-L. Ho, *Phys. Rev. Lett.*, **98**, 180404 (2007); T.-L. Ho and Q. Zhou, *Phys. Rev. Lett.* **99**, 120404 (2007).
- ⁹ Y. Kato, *et al.*, *Nature Phys.* **4**, 617 (2008).
- ¹⁰ A.M. Rey, G. Pupillo, and J.V. Porto, *New J. Phys.* **8**, 161 (2006).
- ¹¹ G.-D. Lin, Wei Zhang, and L.-M. Duan, *Phys. Rev. A* **77**, 043626 (2008).
- ¹² F. Gerbier, S. Foelling, A. Widera, and I. Bloch, arXiv:cond-mat/0701420.
- ¹³ F. Gerbier, S. Trotzky, S. Folling, U. Schnorrberger, J.D. Thompson, A. Widera, I. Bloch, L. Pollet, M. Troyer, B. Capogrosso-Sansone, N.V. Prokof'ev, B.V. Svistunov, *Phys. Rev. Lett.* **101**, 155303 (2008).
- ¹⁴ L. Pollet, C. Kollath, K. Van Houcke, and M. Troyer, arXiv:0801.1887.
- ¹⁵ S. Wessel, F. Alet, M. Troyer, and G.G. Batrouni, *Phys. Rev. A* **70**, 053615 (2004)
- ¹⁶ E. Altman and A. Auerbach, *Phys. Rev. Lett.* **89**, 250404 (2002); S.D. Huber, E. Altman, H.P. Buchler, and G. Blatter, *Phys. Rev. B* **75**, 085106 (2007).
- ¹⁷ C.J. Penthick, and H. Smith, *Bose-Einstein Condensation in Dilute Gases* (Cambridge, New York, 2002).
- ¹⁸ C. Menotti and N. Trivedi, *Phys. Rev. B* **77**, 235120 (2008).
- ¹⁹ J.K. Freericks and H. Monien, *Europhys. Lett.* **26** 545 (1994); K. Sengupta and N. Dupuis, *Phys. Rev. A* **71**, 033629 (2005); J.K. Freericks and H. Monien, *Phys. Rev. B* **53**, 2691 (1996).
- ²⁰ S.-P. Kou and R.-H. Li, *Inter. J. Mod. Phys. B* **21**, 249 (2007); L. Amico and V. Penna, *Phys. Rev. Lett.* **80**, 2189 (1998).
- ²¹ X. Lu and Y. Yu, *Phys. Rev. A* **74**, 063615 (2006).
- ²² M.P.A. Fisher, P.B. Weichman, G. Grinstein, D.S. Fisher, *Phys. Rev. B* **40**, 546 (1989).
- ²³ *Quantum Phase Transition*, by S. Sachdev, Cambridge University Press (1999).
- ²⁴ Private discussion with Ian Spielman.